Design and Safety Assessment of Wearable Transcranial Low-Intensity Pulsed Ultrasound Devices

by

Shiang Qi

A thesis submitted in partial fulfillment of the requirements for the degree of

Master of Science

in

Biomedical Engineering

Department of Electrical and Computer Engineering
University of Alberta

Abstract

Mental illness grow to become one of the most significant issues in the global medical burden. Ultrasound therapy has shown excellent performance in many clinical applications. Some encouraging evidence has shown that transcranial ultrasound stimulation (TUS) has a beneficial effect on relieving symptoms of mental illness (neuropsychiatric disorders). However, the commercially available low-intensity pulsed ultrasound (LIPUS) devices are usually bulky, power-consuming, and not designed explicitly for transcranial stimulation. There is a need for the implementation of a portable LIPUS device suitable for area-constrained embedded applications designed particularly for applying ultrasound stimulation to the brain. To address this need, this study designs and implements an internet of things (IoT) portable LIPUS generation system for TUS application.

The LIPUS generating system is composed of head-mounted transmission equipment, a LIPUS signal driving device, and a mobile application. In the head-mounted transmission equipment, in addition to the necessary accessories and appearance parts, the main components include an ultrasonic transducer, a rubber cap, the ultrasound agents, and an impedance matching circuit board. Studies are carried out to investigate the applicable ultrasound generation characteristic. The driving circuit module, the Bluetooth module, the power module, and the appearance accessories form a LIPUS signal driving module. The ultimate goal of this work is to design a prototype LIPUS generation system that is implemented using discrete components. After verification, the LIPUS generator can work appropriately after manufacture, and can generate LIPUS power from 30 mW to 590 mW (LIPUS intensity from 6.1

mW/cm^2 to 120 mW/cm^2) at the resonant frequency of 1.5 MHz of the transducer.

In addition, there have been a few studies that have estimated the risk of using therapeutic ultrasound. After developing a head-mounted LIPUS device, verification is performed to evaluate possible tissue damage when different intensity levels of LIPUS stimulation are applied through the temple to the brain. Our computer simulations and *in vitro* experiments show that our customized LIPUS devices can safely deliver small doses of low-intensity pulsed ultrasound to the brain through the skull without damage to the contacted skin and inner tissue. When a higher dose of LIPUS is applied to the temple, the skin in contact with the transducer may produce temporarily reversible injury. These results show that this approach has the potential to be used in the treatment of many neurological diseases as a TUS method in the future.

Preface

This thesis is an original work by Shiang Qi. Some parts of this thesis contain published articles that were authored or co-authored. All the author's contributions on the related published articles are listed as follows:

Parts of the content in Chapter 1 section 2 have been published as a review paper in IEEE Transactions on Biomedical Engineering with the title "A review of low-intensity pulsed ultrasound for therapeutic applications." Each author contributed to some content in the manuscript. Shiang Qi was responsible for the literature review of the therapeutic applications of low-intensity pulsed ultrasound in two aspects: soft-tissue regeneration and inflammatory inhibiting. Xiaoxue Jiang, as the first author, was also responsible for organizing the literature from each authors' manuscript, reviewing and writing a rebuttal. The project was conducted under the supervision of Jie Chen.

Parts of the content in Chapter 2 and Chapter 3 of this thesis have been published as a conference paper in the 2018 40th Annual International Conference of the IEEE Engineering in Medicine and Biology Society (EMBC) with the title "Design of a novel wearable LIPUS treatment device for mental health treatment". Shiang Qi is the first author. He conducted all of the experiments, wrote most of the sections, and prepared the manuscript. Shiang also led the work and contributed to reviewing and editing the literature. Yufeng Li contributed to some schematic design and figure editing. Wei Zhang contributed to the investigation of the LIPUS background. The manuscript was reviewed and revised by Yufeng Li and Dr. Jie Chen.

Parts of the content in Chapter 4 of this thesis have been published as a con-

ference paper for the upcoming 2020 42nd Annual International Conference of the IEEE Engineering in Medicine and Biology Society. The title of this paper is "Safety assessment of a wearable low-intensity pulsed ultrasound device for relieving mental illness symptoms". Shiang Qi is the first author as well and responsible for all the experiments and preparing the manuscript. Dr. Jie Chen is the corresponding author.

Dedicated to my parents

Acknowledgements

This thesis was completed under the guidance of my supervisor, Dr. Jie Chen. I would like to acknowledge Dr. Jie Chen for providing me the opportunity to study under his supervision in the BINARY lab at the University of Alberta. The profound professional knowledge, the serious scientific attitude, the rigorous academic spirit, and the untiring and noble morality of him have had a profound impact on me. From the selection of the project to the completion phase of the project, Dr. Chen always gave me careful guidance. Dr. Chen not only helped me set ambitious academic goals but also taught me many truths about life. When I am confused about the thoughts of the research and thesis, Dr. Chen clarified the thoughts for me and guided me with an innovative thought. Here, I would like to extend my most sincere gratitude and heartfelt thanks to Dr. Chen!

In my master's period, I'm honored to work with a bunch of excellent graduate students and post-doctoral fellows at the BINARY Researh lab: Dr. Xiaoxue Jiang, Dr. Yufeng Li, Wei Zhang, Tianlin Yang, Kaining Mao, Ben Flanders, etc. Collaborating with them and making progress together has been a great pleasure.

Finally, I would also like to acknowledge my family for their support. Without their encouragement and support, I would not be what I am today. Thank them for supporting my choice of the research path. I also want to thank my girlfriend for her care and spiritual support. I thank her for all her dedication and sacrifice.

Table of Contents

List of Tables

List of Figures

Abbreviations

BCCAO stands for bilateral common carotid artery occlusion.

BDNF stands for brain-derived neurotrophic factor.

CBT stands for cognitive behavioural therapies.

DA stands for dopamine.

DBS stands for deep brain stimulation.

ECT stands for electroconvulsive therapy.

FDA stands for Food and Drug Administration.

fMRI stands for functional magnetic resonance imaging.

HIFU stands for high-intensity focused ultrasound.

IoT stands for Internet of things.

LIPUS stands for low-intensity pulsed ultrasound.

LIUS stands for low-intensity ultrasound.

MDD stands for major depressive disorder.

MDE stands for major depressive episodes.

MST stands for magnetic seizure therapy.

NDT stands for non-destructive testing.

NE stands for norepinephrine.

NPC stands for neuron progenitor cell.

OL stands for oligodendrocyte.

PCB stands for printed circuit board.

rTMS stands for repetitive transcranial magnetic stimulation.

SATA stands for spatial averaged and temporal averaged.

TRD stands for treatment-resistant depression.

TUS stands for transcranial ultrasound stimulation.

UART stands for universal asynchronous receiver/transmitter.

VNS stands for vagus nerve stimulation.

WHO stands for World Health Organization.

Chapter 1

Introduction

1.1 Depression Background

1.1.1 Introduction of Depression

A substantially increasing population is suffering from mental disorders (depressive disorders and anxiety disorders). Depression, also known as major depressive disorder (MDD), has enormous symptoms [1] including feeling sad and hopeless, bursts of anger, easily irritable, loss of interest or engagement during most or all normal activities sleeping disorders, tiredness and lack of energy, and increased decreased desire for food which lead to weight gain or loss, and others. Although depression may only occur once in a person's life, it may have multiple occurrences for most people. According to a World Health Organization (WHO) report in 2017 [2], MDD is expected to be one of the world's most significant medical burdens and the second-largest cause of death for people between 15-29 years old. This situation has been aggravated because depression can affect people of all ages and all occupations. About 20% of people will experience mental disorders during their youth [3], and 25% of all women will suffer from depression in their lifetime, especially during the pregnancy and postnatal period [4, 5]. Patients can hardly get rid of major depressive disorder because of the high recurrence rates, which are higher than 60% among patients during the follow-up period [6].

Moreover, at its most severe, patients may commit suicide (with suicidal ideation

between 10 to 15%) [7]. According to the WHO report in 2017, there are an estimated 788,000 people who died as a result of suicides in 2015, and there are more suicide attempts [2]. In Canada, major depressive episodes (MDE) have made a considerable contribution to the cause of disability, with an annual prevalence rate of 4.7% in the year of 2012 [8].

1.1.2 The Pathogenesis of Depression

Although MDD has become one of the arduous medical burdens in the world and is affecting nearly one-fifth of the population worldwide [9], the pathogenesis (molecular and cellular mechanisms) of MDD has not been fully understood. Due to our limited understanding of the pathogenesis of MDD, the search for targeted drugs and specific treatment methods has been severely hampered.

In studying the pathology of depression, researchers have proposed various hypotheses. These hypotheses try to explain the cause of depression through different molecular or cellular mechanisms, helping future researchers to screen for targeted drugs. There are different hypotheses [10, 11] (the academic term might vary from different literature), including the neumonoamine hypothesis, the neurogenesis hypothesis, the neurotrophic hypothesis, and others. The first hypothesis of MDD was proposed in the 1960s. This hypothesis assumes that the main symptom of depression is due to insufficient monoamine activity in central synapses in the brain [12]. The hippocampus disturbed forms the theory of the neurogenesis hypothesis of depression [13]. The decrease in the proliferation rate of exogenous neural neuron progenitor cells (NPCs) may be the main factor for abnormal hippocampal function, which may be caused by external pressure [14]. Studies have also shown that some neurotrophic factors, such as brain-derived neurotrophic factor (BNDF), play an essential role in the pathology of depression. These established another neurotrophic hypothesis of depression: shortage neurotrophic support, atrophy of neurons, reduced hippocampal neurogenesis, and glial loss derive the development of depression [15].

The information about some mainstream hypotheses of MDD can be found in Table 1.1. The pathological cause of depression has been investigated in recent years with enormous emerging hypotheses, like the white matter hypothesis of depression [16], the glucocorticoid hypothesis of depression [17], the inflammatory hypothesis of depression [18], the enzymes hypothesis of depression [19], the mitochondrial hypothesis of depression [20], along with others. Due to space limitations, we will not introduce these emerging hypotheses in detail in this chapter.

Table 1.1: Hypotheses of major depressive disorder.

Hypothesis	**Description**
Monoamine hypothesis	Depression is caused by insufficient monoamine neurotransmitters, including serotonin, norepinephrine (NE), and dopamine (DA) [21].
Neurogenesis hypothesis	Depression is caused by disturbed hippocampal function. External stress diminishes the proliferation rate of NPCs and reduces survival by inhibiting the growth and development of neurons.
Neurotrophic hypothesis	Depression is caused by reduced neurotrophic factors (BDNF), neuron atrophy, reduced hippocampal neurogenesis, and glial loss.
Glucocorticoid hypothesis	Corticosteroids affect neurotransmitters, which in turn affects depression induced by external stress.
White matter hypothesis	Depression is caused by abnormal cellular myelin and oligodendrocytes (OLs).
Inflammatory hypothesis	Inflammation can affect depression by affecting neural transmission, neural circuits, and causing behavioral changes.

Various components such as mood, behavior, and cognition, all of which may involve changes in nerves or cytokines, make up the complex, multifaceted nature of depression [10]. Hasler *et al.* encourages researchers to use biomarkers (for the instance neuroimaging and neuroendocrine tests) to make accurate predictions of factors that respond to depression interventions [10]. Identifying reliable predictors

will help better explain the causes of depression and develop effective treatments.

1.1.3 Treatment Approaches for Depression

Depressive and anxiety disorders have various treatment methods. Treatment selection in mental disorders includes psychological interventions, pharmacological interventions [22], a combination of psychotherapy and pharmacotherapy [23], as well as other emerging intervention methods like exercise [24, 25].

Antidepressant, a type of medication for MDD treatment, is one of the significant branches of pharmacological interventions. The history of antidepressant treatment can be traced back to the 1950s. Freis *et al.* applied a high concentration of reserpine to hypertensive patients, which causes a series of mental illness complications in the patient [26]. In the experiments, depression disappears among some patients after discontinuing reserpine.

Some antidepressant treatments are considered to have an increased risk for discontinuation of medicine, leading to easy recurrence [27], which is also named antidepressant discontinuation syndrome. Besides, approximately 50% of patients with depression respond to current clinical antidepressant treatments [28], which casts a shadow over the development of new antidepressant treatments.

Compared with medication, people with depression usually prefer psychotherapy because it can provide patients with a positive and healthy mentality for reducing depression symptoms [29]. Furthermore, an ocean of psychological interventions has been developed for patients with antidepressant-resistant depression [30]. However, cognitive behavioral therapies (CBT) [31], as a commonly used high-intensity psychological intervention, shows no evidence to be as efficient as the pharmacological interventions, especially in patients with severe depressive symptoms [32]. Some literature reports that the combined treatment of CBT and pharmacotherapy is more effective but more expensive than antidepressant treatment for patients [22, 33]. Nevertheless, the current treatment method is still ineffective for a large portion of patients. There-

fore, researchers aim to discover an alternative treatment method to treat depression cost-effectively.

In recent decades, neurostimulation, as an emerging intervention approach for treatment-resistant depression (TRD), has proved to have great potential and has begun to attract the attention of a considerable number of researchers. Neurostimulation is a physical stimulus applied to the brain. Nerve stimulation activates intracranial nerve cells inside of the brain by the stimulation of current, magnetic field or ultrasound field. Currently, accessible neurostimulation techniques include electroconvulsive therapy (ECT), repetitive transcranial magnetic stimulation (rTMS), magnetic seizure therapy (MST), vagus nerve stimulation (VNS), deep brain stimulation (DBS) and other interventions being studied [34]. Some primitive information of these significant neurostimulation intervention methods can be found in Table 1.2.

ECT has firstly been used for psychiatric disorders since 1930 and is ideal for severely depressed patients with suicidal ideation [35]. ECT intervention employs a brief electrical stimulation to the patient's brain area. The patient must be anesthetized during the stimulation to avoid motor convulsions [36]. rTMS treatment applies a magnetic field to a target deeper brain structure, which is then stimulated by the generated electric pulse through the cortex [37]. Unlike ECT, the non-invasive rTMS is much safer because it does not induce seizures nor need patients to be anesthetized [34]. MST, as a combined form of ECT and rTMS, uses the magnetic field to induce a seizure. Some beneficial of MST includes the ability to generate focal stimulation to the brain compared to ECT, and the ability to deliver much higher intensity compared to rTMS [38]. VNS was originally invented for epilepsy treatment; its stimulating effect on the vagus nerve makes it very promising in the therapeutic application of depression [39]. An electrode connected to a pulse generator is placed at the left vagus nerve, which carries out the brain stimulation through a low-frequency pulsed current wave [40]. VNS can be treated as an adjuvant therapy intervention for patients with chronic or recurrent major depression for long-term use. Another

invasive method to treat TRD patients is DBS. This intervention places electrodes deep in the brain and is driven by a pulse signal. DBS applies electrical impulses to regulate brain activity. The potential mechanism of DBS is still under-investigated though several controlled trials have confirmed its changes in brain activity [41]. The possible side effects of VNS and DBS are associated with electrodes implantation under the skin [42].

1.2 Ultrasound and Its Therapeutic Application

1.2.1 Introduction to Ultrasound

Ultrasound is a type of longitude sound waves with frequency higher than the upper limit of the human hearing range (20 kHz). Longitude sound waves mean that when exposed to longitude ultrasound waves, the components (molecules, cells, soft tissues, and others) in the medium will oscillate around a fixed point rather than moving in the direction of the wave's propagation. The source of ultrasound, in the application of non-destructive testing (NDT) and medication, is usually a piezoelectric transducer. Just like the fundamental level of sound, ultrasound wave contains *"mechanical energy transmitted by longitude sound waves at increasing frequenc"* [43].

As a result of the high frequency, ultrasound has several characteristics. The first is that the power of ultrasonic waves is much higher than that of ordinary sound waves so that they can be used for cutting, welding, drilling, etc. In addition, because of its high frequency, as well as the short wavelength and less severe diffraction, it has the property of excellent directivity. Ultrasound detection is commonly used in industry and medicine.

Ultrasonic waves are widely used to detect objects and measure physical distances (like sonar). Meanwhile, the ultrasonic therapeutic application has a long history in medicine with variety used [44]. Ultrasound has been demonstrated as a useful tool in medical imaging and applied in the physiotherapy treatment. There is a variety of

ultrasound systems to choose from, from ultra-miniaturized devices (Lumify, Philips) [45] to large systems, including multimodal ultrasound systems.

Therapeutic ultrasound refers to any medical application that applies ultrasound for therapy [46]. Typical ultrasound devices transport ultrasonic waves with frequencies from 20 kHz and going up to several gigahertz. However, in general, the frequency range people choose to use for the therapeutic application is between 1 to 3 MHz [47].

Early in the 1920s, Wood *et al.* [48] and Harvey *et al.* [49] first explored the feasibility for the physical and biological effects of high-intensity ultrasound as a non-invasive therapy treatment method. They concluded that the ultrasound wave heats the medium cells which absorb the waves and accelerates chemical reactions (detail of the chemical reaction). When the tissue temperature rises between 40 to 45°C for at least 5 minutes, a significant biothermal effect can be carried out [50]. Gallo *et al.* illustrated that both continuous and pulsed high-intensity ultrasound waves could lead to a tremendous temperature increase with limited biothermal effect, which is difficult to have practical significance in clinical application [51].

For these reasons, in recent years, the non-thermal effects (cavitation effects, acoustic streaming, and mechanical stimulation [47]) attributed by low-intensity ultrasound (LIUS), has been investigated and promoted the development of a variety of therapeutic applications [52]. The non-thermal effects, sometimes now referred to as a micro-thermal effects, can cause therapeutic effects with no apparent thermal accumulation in biological tissue [50].

1.2.2 Low-intensity Pulsed Ultrasound

Ultrasonic waves can be divided into transverse waves and longitudinal waves according to the form of vibration. According to the frequency, it can be divided into low frequency (20 - 40 kHz), intermediate frequency (100 kHz to 1 MHz), high and ultra-high frequency (above 10 MHz up to 70 MHz). Furthermore, ultrasound can be classified into continuous wave and pulse wave according to the waveform modulation.

Low-intensity pulsed ultrasound (LIPUS) is a special type of intermediate frequency, longitudinal ultrasound signals which consist of a series of discontinuous ultrasound signals [53]. The spatial averaged and temporal averaged (SATA) intensity of LIPUS signal used in physiotherapy is usually lower than 1 W/cm^2. An intuitive way of expressing the spatial and temporal behavior of the ultrasonic beam is to plot the pressure distribution versus time at a fixpoint of the transmission medium. The important parameters of the LIPUS wave include the frequency, repetition rate, and SATA intensity. As shown in Figure 1.1, the frequency represents the number of periodic changes in a sine wave. The repetition rate represents the number of times the ultrasound periodically starts and stops. The amplitude of the sine wave reflects the magnitude of the intensity. SATA intensity involves a time average of the intensity of all propagation pulses and intervals. The example modulated LIPUS signal presented in Figure 1.1 has a parameter of 1.5 MHz frequency, 1 kHz repetition rate with 20% duty cycle. During the "on time" period (200 μs), it contains 300 sine wave pulses, where each pulse has a period of $\frac{1}{1.5}\mu s$.

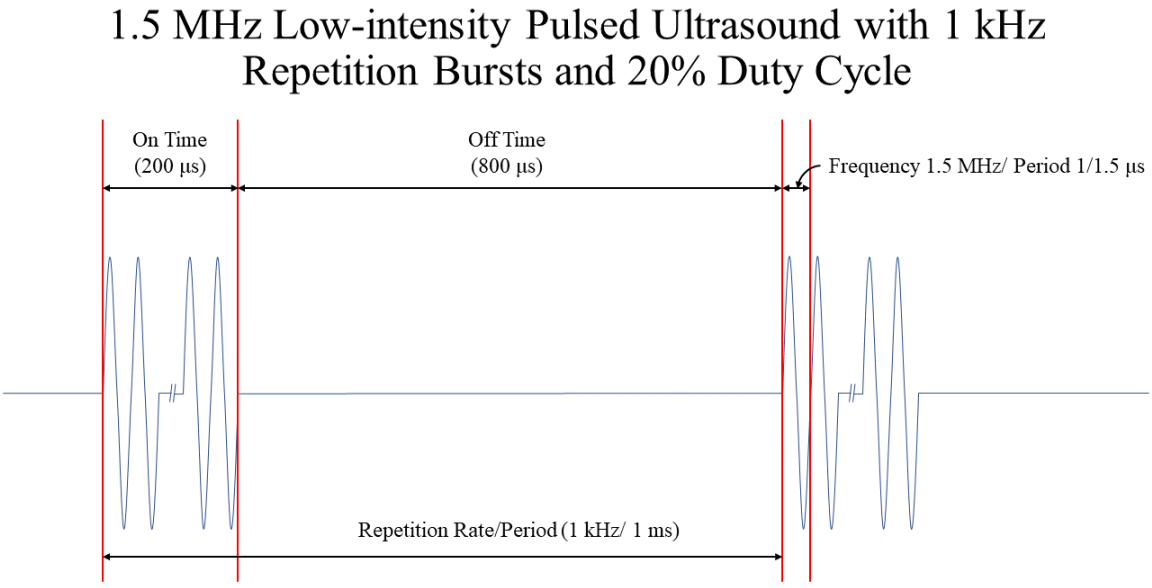

Figure 1.1: Modulated LIPUS waveform pattern.

It may seem strange to specify the acoustic intensity other than signal amplitude or pressure when we are discussing the power of the biological effects of ultrasound. However, when discussing the biological effects of ultrasound, it is helpful to use intensity (SATA intensity or spatial peak temporal average intensity, SPTA). The relationship between the intensity I at a position of propagation medium and the ultrasonic pressure amplitude P is:

$$I = \frac{P^2}{2\rho c} \tag{1.1}$$

In this equation, ρ is the density of the propagation medium, and c is the propagation velocity of the sound in the medium. The product of ρc is the acoustic impedance of the propagation medium. Therefore, based on Equation 1.1, the acoustic intensity is proportional to the square of the sound pressure. However, the intensity is complicated because it varies over time and from point to point. When we are considering the temporal difference of the pulsed ultrasound wave, intensity might be averaged over a half cycle (max intensity or I-max), over the pulse duration (pulsed average intensity), or over the time from the start of one pulse to the next (time average intensity). The relationship between pulsed average intensity $I_{\mathbf{PA}}$ and time average intensity $I_{\mathbf{TA}}$ is:

$$I_{\mathbf{TA}} = I_{\mathbf{PA}} \times \mathbf{DF} \tag{1.2}$$

where **DF** denotes the duty factor. To avoid measuring the intensity from point to point, the spatial average (SA) intensity is employed for diagnostic instruments and medical utilities. The relationship between the spatial average and the time average (SATA) intensity and the acoustical power is:

$$I_{\mathbf{SATA}} = \frac{W}{A} \tag{1.3}$$

where A denotes the cross-sectional area of an ultrasonic beam. Compared to higher-

intensity ultrasound, the goal of a low-intensity design is to alleviate the thermal effect or to minimize the thermal effect [54]. The non-thermal effects refer to that the tissue has no apparent thermal accumulation. Possible mechanisms that might be associated with the non-thermal effects include cavitation, acoustic streaming, and standing waves [46]. Under the propagation of the mechanical vibration effect of ultrasonic waves, micro-bubbles will be generated in gas-containing medium (blood or brain tissues) because of the cavitation. These small bubbles will change the osmotic pressure in the cell, and changes in the concentration of calcium ions may affect the behavior of the cell [55]. However, cavitation effects are not all beneficial. High-pressure bubbles may cause high pressure or high temperature in the cells, causing a series of violent cavitation effects [50].

Since the 1950s, LIPUS has been widely applied in various therapeutic applications including bone fracture healing [56], ultrasound transdermal drug delivery [57], soft-tissue regeneration [54], inhibition of inflammation [58], and non-invasive neuromodulation [47]. Figure 1.2 is a diagram exhibiting the different therapeutic applications of LIPUS.

Early research on the use of ultrasound for bone healing dates back to 1952 [59]. Since then, more and more research evidence supports the idea that LIPUS can promote bone healing. Therapeutic LIPUS is commonly used daily in bone healing treatment with a long duration. The commonly used therapeutic LIPUS stimulation is characterized by a frequency of 1.5 MHz, an intensity below 1 W/cm^2, and a duty cycle of 20% [60].

As early as in 1990, Enwemeka *et al.* studied the potential effects of low-intensity ultrasound on healing tendons [61]. By comparing the mean tensile strength, tensile stress, and energy absorption capacity, numerous studies indicated that sonication at lower intensities could promote the early healing process of tendon even though some literature showed some different opinions [62–64]. The therapeutic effects of LIPUS on fibroblasts, myoblasts, epithelial cells, and chondrocytes have led to other

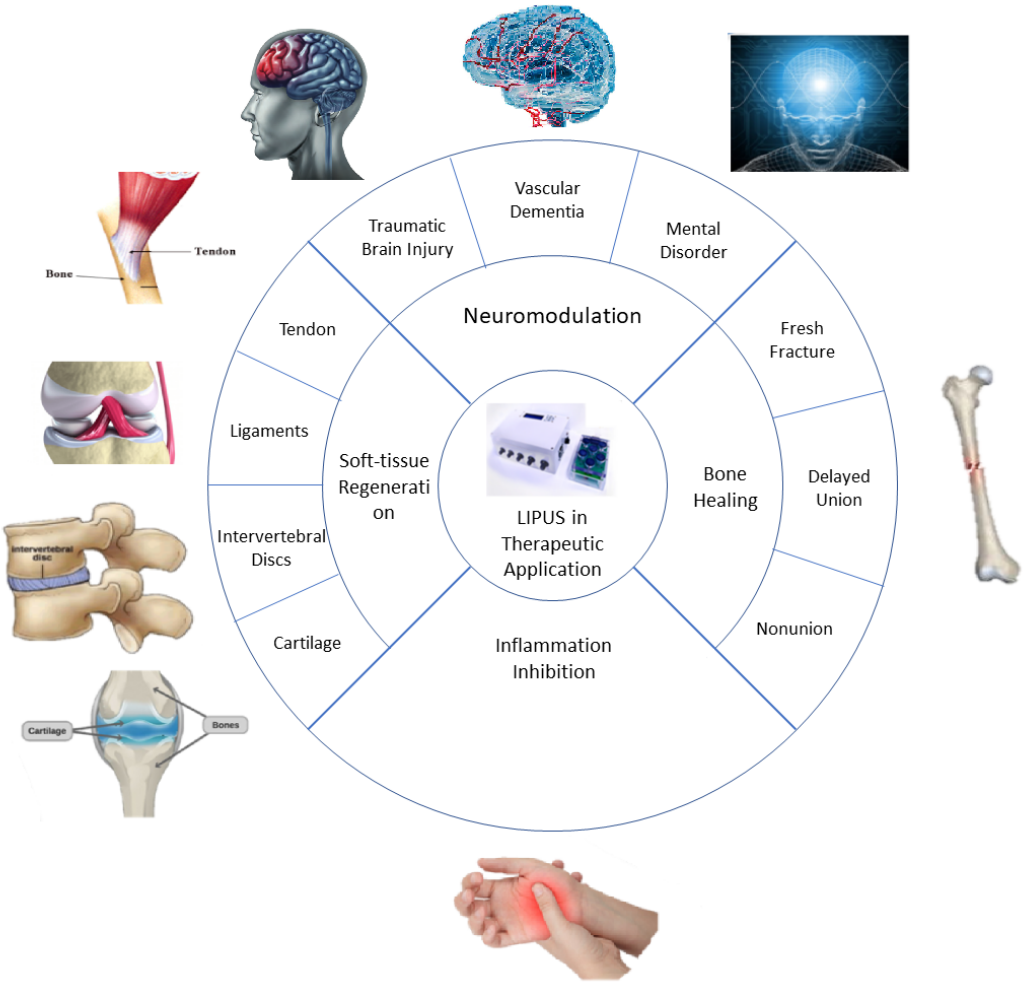

Figure 1.2: Different therapeutic applications of LIPUS.

applications of soft tissue regeneration, such as ligament healing, intervertebral disc absorption, and cartilage recovery.

Inflammation is a typical response during the healing process. Nevertheless, when the inflammatory response lasts for too long, it can affect the viability and transcriptional activities of the regeneration process [65]. Researchers find that under the action of the LIPUS, it is possible to counterbalance the pro-inflammatory cytokines and obtain a better treatment effect.

1.2.3 Feasibility of Ultrasound for Depression

Transcranial ultrasound stimulation (TUS) was considered to have considerable potential for mental diseases because of the thermal effects of high intensity ultrasound. Nevertheless, the non-thermal neuroprotective and neuromodulatory effects of LIPUS has raised a great interest in recent years. The neuromodulation and neuroprotective effects of LIPUS have been confirmed *in vivo* in many other studies, indicating its potential application prospects.

Focused ultrasound with low-intensity dose has been investigated for the potential of mental illness treatment. Together with functional magnetic resonance imaging (fMRI) guided techniques, focused ultrasound has been reported to have a beneficial effect on depression patients in comparison to the control group [66, 67]. However, due to its characteristics, focused ultrasound tends to accumulate too much energy when overlapping stimuli. It may cause minimally invasive thermal damage to the skin. Instead, low-energy pulsed ultrasound can avoid thermal injury to the greatest extent under the same therapeutic effect.

In 2008, a research team led by Muratore, Tyler *et al.* found that using relatively low-intensity ultrasound to stimulate hippocampal cultures and mouse brains *in vitro* can directly trigger action potentials and synaptic transmission of central neurons, as well as the changes in the concentration of Ca^{2+} and Na^{+} between cells [68].

Chen *et al.* demonstrated that LIPUS treatment significantly alleviates the ischemic brain damage and improves the neurological and behavior function performance in adult mice [69]. Based on the molecular-level analysis, LIPUS treatment helped inhibit the neuronal cell apoptosis and downregulation of brain-derived neurotrophic factor (BDNF) [69]. Huang *et al.* applied short-duration LIPUS treatment on the bilateral common carotid artery occlusion (BCCAO) mice [70]. The *in-vivo* study indicated that the BDNF level has significantly increased in mice after the treatment. Another *in-vivo* study showed that LIPUS treatment could significantly

improve behavior and histological results in traumatic brain-damaged mice [71].

Guo published results indicated that LIPUS is able to significantly ameliorate depressive behaviors in mice after exposure to repetitive restraint stress [72]. In-vitro results also suggested that possible mechanisms for the beneficial effects of LIPUS on depression are the promotion of neurogenesis and an increase of BDNF [72]. Zhang *et al.*'s study also demonstrated that the application of low-intensity ultrasound is able to promote the BDNF expression in the left hippocampus. Some researchers concluded that mechanically sensitive ion channels, after ultrasound stimulation, might be the key mediators of these nerve activation [73, 74].

In addition, depression often occurs together with anxiety. Depression patients are often accompanied by symptoms of anxiety. Some studies demonstrate that ultrasound stimulation can alleviate the anxiety symptoms with short time pulsed stimulation. Erfani *et al.* investigated the effects of ultrasound stimulation on anxiety-like behavior in mice models [75]. Experimental results demonstrated that ultrasound has some anxiolytic effect on mice, including increasing the time for mice to open their arms. Rezmik *et al.* delivered low-intensity TUS (30 secs, 500 kHz frequency, 40 Hz repetition frequency) to mild and moderate depressive adults [76]. Worry symptoms in these subjects sensitively decreased in the TUS group while depression score has not changed significantly. Legrand *et al.* demonstrated that applying TUS on the infralimbic cortex leads to diminished anxiety-like behaviors and some of the depression-related parameters, as well as the activation effects of some targeted brain region [77]. Transcranial ultrasound neurostimulation shows the potential clinical ability to alleviate anxiety and depression comorbid disorders in recent years.

However, the development of LIPUS in clinical trials for the treatment of mental illness (brain injury, Alzheimer's disease, and mental disorders) has progressed significantly slowly. The safety of the LIPUS treatment on neuromodulation has barely been investigated. Few studies have evaluated the possible adverse effects of LIPUS therapy [57, 78]. However, these studies are insufficient to draw conclusions about

the safety of LIPUS therapy for human brain stimulation. In this study, we designed a novel head-mounted LIPUS therapy system and assessed the safety of this device.

1.3 Thesis Scope and Outline

This thesis is organized into five chapters to present a novel portable low-intensity pulsed ultrasound headband device and inspect the clinical safeness of the device. This manuscript is structured in the following manner. Chapter 1 introduces the current research on depression, some existing treatment options for depression, and the pathogenesis of depression. Chapter 1 also reviews the research progress for therapeutic ultrasound and the possibility of using low-intensity ultrasound for mental illness treatment.

Chapter 2 focuses on the low-intensity pulsed ultrasound system design. This chapter includes a detailed introduction to the ultrasonic transducer characteristic analysis, impedance transform circuit design, signal generator circuit design, and communication module design. We also designed a software system that can seamlessly interface with the hardware system.

There is no specific ultrasound transducer cap that exists on the market to aim treatment via temples. In Chapter 3, we design a replaceable cap for the ultrasound transducer and a headphone for transcranial stimulation usage. Four identical ultrasound transducers, driven by the LIPUS device, were used in the experiment to examine the transmission sound intensity with the cap design and different ultrasound coupling agents (sham group, Milli-Q water, transformer oil, and ultrasound gel). We obtained the best material for the ultrasound output system through data analysis and curve fitting.

Chapter 4 investigates the idea of using our manufactured LIPUS system for mental illness treatment through the stimulation of the human brain. Both computer simulation study and *in-vitro* brain tissue-mimicking phantoms experiment are conducted to verify the feasibility and safety.

Chapter 5 summarizes the entire thesis and describes a slice of possible future work.

Table 1.2: Summary of the major neurostimulation intervention methods.

	Description	**Advantages**	**Disadvantages or Side Effects**
ECT	A brief electrical stimulation induced by electrodes placed on the scalp. The electrical pulse activates a general area of the brain to induce seizures.	ECT is efficient for patients with severe depressive symptoms.	Side effects include restricted venue, anesthesia, and possible short-term amnesia; High recurrence rates within the first year after receiving ECT.
rTMS	A brief magnetic stimulation induced by the electromagnetic coil placed near the scalp. rTMS can directly activate the target deeper structures.	rTMS has the ability to produce focus stimulation to deeper structures like the hippocampus and thalamus; This therapy is safer than ECT and does not require patients to be anesthetized.	The standardization of the parameters of rTMS is still under-investigated.
MST	MST is a combined intervention of ECT and rTMS, which uses magnetic stimulation to provoke a seizure in the target brain area.	MST can target and stimulate certain areas of the brain; MST has a higher intensity capacity to provoke a seizure.	Like ECT, patients must be anesthetized and treated in hospital.
VNS	VNS stimulates the brain indirectly by stimulating the vagus nerve by implanting a pulse generator subcutaneously.	VNS can be used as an adjuvant therapy intervention for patients with chronic or recurrent major depression for long-term use.	Most side effects of VNS are generated because of invasive surgery to place the electrode; The common postoperative syndrome includes voice alteration, dyspnoea, and cough.
DBS	DBS uses electrical impulses to regulate brain activity with electrodes placed under the skin.	DBS can target and stimulate certain areas of the brain.	Similar to VNS, most of the side effects are associated with a high risk of neurosurgery; Other side effects include lightheadedness, insomnia, and psychomotor changes

Chapter 2

Design of the Wearable Low-intensity Pulsed Ultrasound Therapy System

2.1 Design Specification Overview

Figure 2.1: Major elements of the LIPUS therapy device proposed in [79]

The portable LIPUS system consists of a software system for control and a hardware device for generating ultrasound. The hardware part includes an ultrasound transducer, impedance matching circuit, and a headphone-style device with LIPUS

transmission. The major parts of the system are shown in Figure 2.1. This ubiquitous and portable LIPUS therapeutic device allows patients to receive treatment wherever they are. In addition, it can be developed into an Internet of Things (IoT) device to enable intelligent identification, location, tracking, and supervision of the prescription (clinicians could control and monitor patients' treatment remotely via the internet). In the system-level design shown in Figure 2.1, the app on the smartphone remotely passes the psychiatrist's prescription to the LIPUS device via Wi-Fi and Bluetooth. The device can send reports to the psychiatrists about whether patients follow the prescription or not. The therapeutic procedure involves applying LIPUS stimulation to the pterions area, also known as the temple area (the junction between the parietal bone, the temporal bone, the sphenoid bone, and the frontal bone) through a flat transducer for a certain time each day. The clinician can change the ultrasound intensity (from 6.1 mW/cm^2 to 120 mW/cm^2) and the treatment cycle (how often do patients need to receive treatment in a certain amount of time, e.g., 5 minutes per day). Ultrasonic waves can transmit through the skull and excite the cerebral nerves.

Typical LIPUS parameters for therapeutic applications are operated at 1-3 MHz frequency, but the SATA intensity should not exceed 1 W/cm^2 SATA. A duty cycle of 20% at 1 kHz repetition bursts is commonly used [47, 49]. Our recent published results have shown that a 1.5-MHz LIPUS wave with intensity lower than 50 mW/cm^2 could be tolerated by animals nerves and soft tissues [72]. Therefore, the objective of this study is to design a remotely controllable LIPUS system that produces a 1.5-MHz LIPUS signal with an intensity lower than 200 mW/cm^2. The ultrasound generation is turned on for 200 μs and off for 800 μs in a loop (20% duty cycle of 1 kHz repetition rate). This LIPUS generator is equipped with a headband and control software that is able to monitor the therapy and modify the therapeutic intensity remotely. The design of the headband will be discussed in Chapter 3.

In this chapter, we propose a LIPUS system design with a wearable characteristic from the following aspects. First, research concerning the ultrasound transducer char-

acteristic is carried out to pursue optimal ultrasound generation techniques. Then, the design of the three main components, which are the impedance transform network, the signal generator network, and the Bluetooth control network, is discussed in detail. Together with the Bluetooth control module, an Android software system is presented and shortly introduced. The design specifications of this LIPUS treatment system are shown in Table 2.1.

Table 2.1: Parameters and specification of low-intensity pulsed ultrasound device.

Parameters	
SATA Power	$30 - 590mW$
Mode of Operation	Pulsed wave
Effective Area	4.91 cm^2
Pulsed Center Frequency	1.5 MHz
Pulse Duration	200 μs
Duty Cycle	20 %
Pulse Repetition Frequency	1 kHz
Estimate SATA Intensity	6.1 - 120 mW/cm^2 (61 - 1200 W/m^2)
Peak Rarefactional Pressure at Specimen	0.030 - 0.133 MPa

2.2 Transducer Characteristic

The 1.5 MHz ultrasound transducers are longitudinal wave transducers fabricated by APC International, Ltd, Mackeyville, USA. The incident wave is perpendicular to the surface. Piezoelectric crystal 880 developed by APC has a piezoelectric charge constant d33 of 215 m/V, frequency constants Nt of 2110 m/s, and a mechanical quality factor of 1000, with 25 mm outside diameters and a 12.5 mm length. The larger the charge constant d33 is, the better the emission performance of the piezoelectric, the stronger the vibration, and the ultrasound are [80].

The transducer consists of a piezoelectric crystal, a closed-cell foam, and some bus bar wire, which are wrapped inside of an aluminum cup with some low viscosity epoxy

adhesive. The architecture of the ultrasonic transducer is illustrated in Figure 2.2. The radius of the aluminum cap is 25 mm, which equals to 4.91 cm^2 effective area.

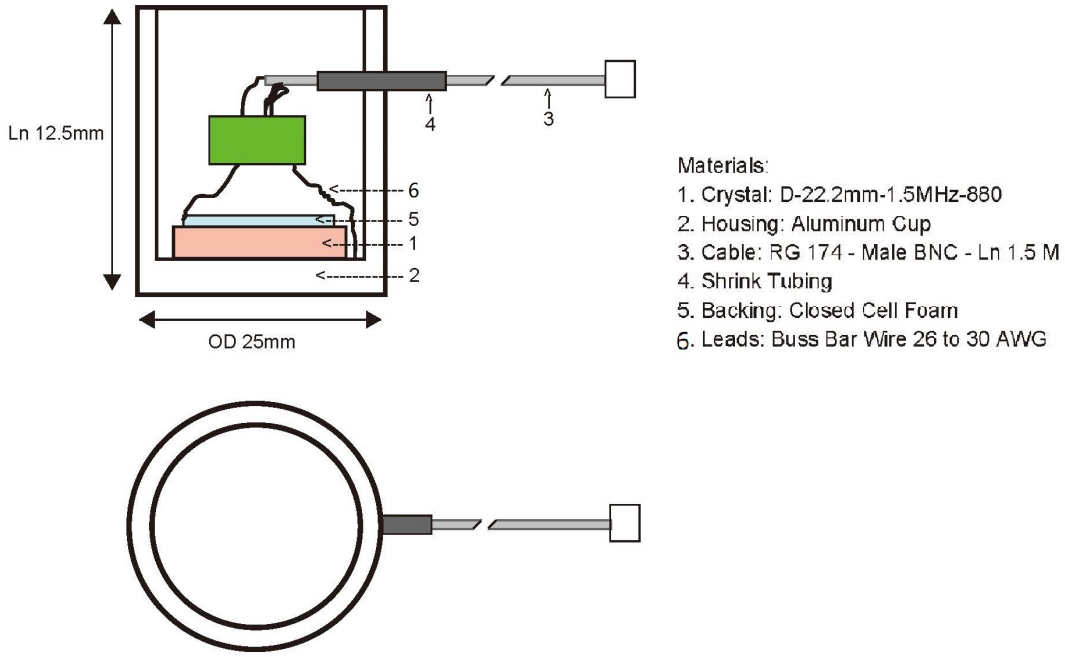

Figure 2.2: Structure of the ultrasound transducer.

An electrochemical measurement station (SP-220, BioLogic Inc., Seyssinet-Pariset, France) is used to measure the transducer characterization. The transducer impedance characterization is demonstrated in Figure 2.4. The excitation signal mode is a single sine wave which has an amplitude from 500 mV to 2500 mV. The measurement frequency range scans from 1 MHz to 2 MHz with 200 linearly spacing points. The measurement station waits from 0.5 periods before each frequency to make another measurement. Each point is the average value of 20 measures per frequency. Figure 2.3 is the photograph of the measurement station and the proposed setup for measuring ultrasound transducers.

In Figure 2.4, these curves consist of the impedance magnitude and impedance phase of the transducer from the several measurements of piezoelectric transducers. At the desired resonance frequency of 1500019.3 Hz (which is the closest frequency to

Figure 2.3: Photograph of the proposed setup for measuring the transducers' characterization.

1.5 MHz), the transducer has an impedance spectroscopy of 14.51 Ohm magnitude and negative 70.68-degree impedance phase. However, for some fabrication reasons, the real resonance frequency, which should have minimum magnitude value and 0-degree impedance phase, lies between 1.5226 to 1.5276 MHz.

We proposed a simplified circuit model in Figure 2.5, which can effectively simulate the piezoelectric transducer when it operates for a narrow bandwidth (fixed at 1.5 MHz). As shown in Figure 2.5, the proposed model connects a resistor and a capacitor in parallel. The relationship among the transducer impedance Z_{load}, the equivalent

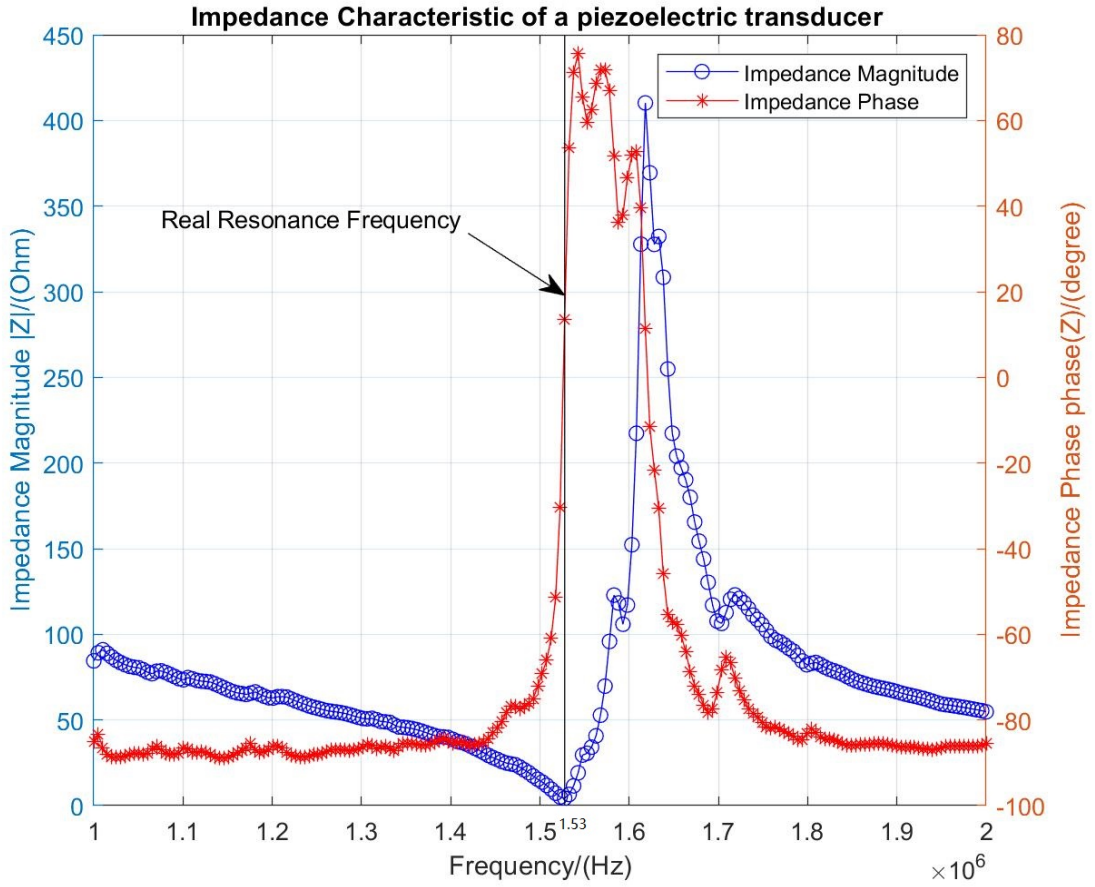

Figure 2.4: Impedance magnitude and impedance phase of a piezoelectric transducer.

resistance, and the equivalent capacitive reactance can be represented as:

$$Z_{load} = \frac{R_{eq}}{1 + j\omega R_{eq} C_{eq}} \tag{2.1}$$

where ω denotes the resonant angular frequency. From Equation 2.1 the relationship between the magnitude and the phase of the complex impedance follows that:

$$\begin{cases} |Z_{load}| = \frac{R_{eq}}{\sqrt{1+(\omega R_{eq} C_{eq})^2}} = \frac{R_{eq}}{\sqrt{1+(\tan(\angle Z_{load}))^2}} \\ \angle Z_{load} = \arctan(-\omega R_{eq} C_{eq}) \\ Z_{load} = |Z_{load}| e^{j\angle Z_{load}} \end{cases} \tag{2.2}$$

Measured magnitude and phase value from the impedance characteristic curves in Figure 2.4 is then substituted to compute the circuit parameters R_{eq} and C_{eq}.

!ht

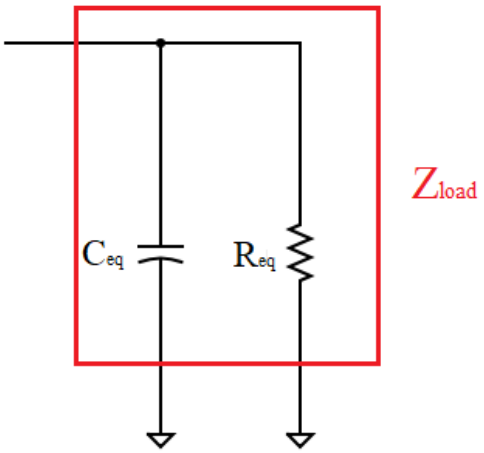

Figure 2.5: Proposed narrow-bandwidth circuit model consisting of a resistor and a capacitor

Take the measurement value at the frequency point of 1500019.3 Hz as an example. The magnitude of the load impedance is 14.511936 Ω, and the phase of the load impedance is $-70.681984°$ from Figure 2.4. Substituting these values into Equation 2.2, We derive the following expressions:

$$\begin{cases} |Z_{load}| = \frac{R_{eq}}{\sqrt{1+(\tan(-70.681984°))^2}} = 14.511936 \\ \angle Z_{load} = \arctan(-\omega R_{eq} C_{eq}) = -70.681984° \end{cases} \tag{2.3}$$

From which, the equivalent resistance R_{eq} is around 43.87Ω, the equivalent capacitance C_{eq} is around $6.90\mu F$. Other sets of data are obtained at different frequency points (f = 1.4974899 MHz, f = 1.5025094 MHz, etc.) The results are all determined using Equation 2.2. The results are summarized in Table 2.2

Although the real resonance frequency of the fabricated transducers is 1.5 MHz, the real equivalent resistance and capacitance will be at some point between 1.4974899 MHz and 1.5000193 MHz. The real equivalent value would be more closed to the calculated equivalent value of 1.5000193 MHz because the absolute distance between 1.5000193 MHz and the real resonance frequency is much closer. Therefore, the equivalent resistance and capacitance are approximated as 44 Ohm and 6.8 nF.

Table 2.2: Calculated equivalent resistance R_{eq} and equivalent reactance X_{eq} at different frequency points.

Frequency/ Hz	**Magnitude (|Z|)/ Ohm**	**Phase (∠Z)/ deg**	**Equivalent Resistance/ Ohm**	**Equivalent Capacitance/ Farad**
1.4874411×10^6	19.256102	-75.890625	78.99170	5.389×10^{-9}
1.4924606×10^6	17.270826	-74.670883	65.32991	5.955×10^{-9}
1.4974899×10^6	15.391371	-71.751869	49.15285	6.558×10^{-9}
1.5000193×10^6	14.511936	-70.681984	43.86773	6.900×10^{-9}
1.5025094×10^6	13.759077	-68.782333	38.01774	7.177×10^{-9}
1.5075388×10^6	11.800703	-65.714378	28.69223	8.155×10^{-9}
1.5125583×10^6	9.5798788	-60.667797	19.55586	9.576×10^{-9}

2.3 Circuit Integration and Layout

The architecture of the LIPUS generation device follows the idea of our previous research [81]. The system can be divided into three modules (control module, signal generation module, drive module), as shown in Figure 2.6.

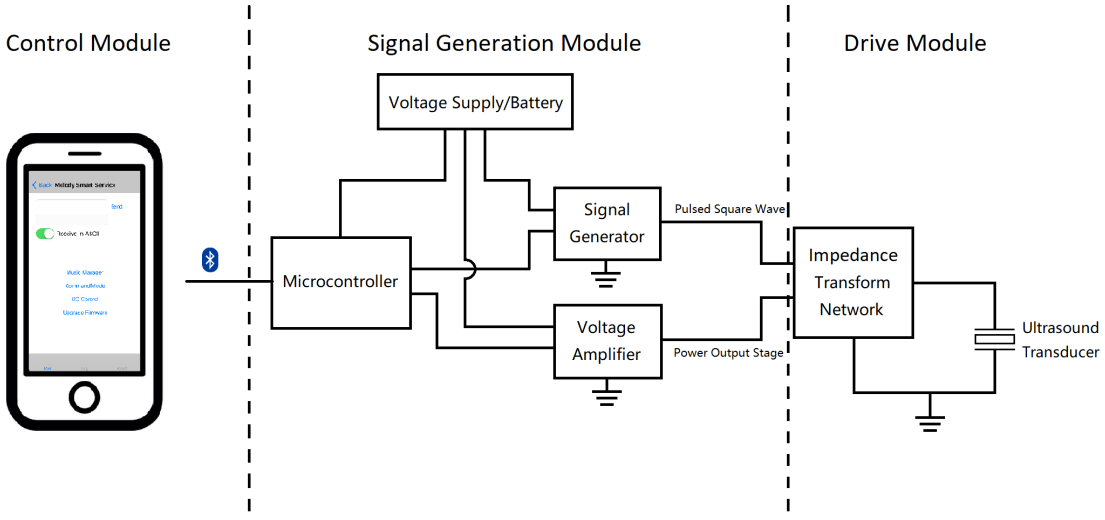

Figure 2.6: Diagram of a LIPUS system

- The control module composes of mobile software (Android platform), a Bluetooth communication chip, and a microcontroller. The mobile app sends a series

of numbers which encode the therapy duration time and intensity level of the LIPUS treatment to the Bluetooth chip. Then, the Bluetooth chip communicates with the microcontroller via the Universal Asynchronous Receiver/Transmitter (UART) interface and decodes the message to obtain the information.

- The design of the signal generation module follows the basic ideas of our previous research [81]. However, we redesign the circuit level layout and change the way the signal is controlled. The microcontroller controls the signal generator to produce LIPUS signal with variable frequency, duty cycle, repetition rate, and duration time. On the other hand, the microcontroller regulates a digital potentiometer to provide the desired voltage, which amplifies the LIPUS signal. The power output stage circuit is designed to provide sufficient current for the LIPUS signal to drive the transducer.

- The third is the drive module, which consists of an impedance transform network and two ultrasound transducers. The function and details of the impedance transform network are discussed in the following subsections, and the circuit design schematic of this module is illustrated in Figure 2.7. The inductive component is implemented by a transformer. The impedance transform network is implemented on other boards that are placed inside the headband due to the large inductor and capacitor values.

2.3.1 Impedance Matching Network

Impedance transformation is a useful technique in power applications. It is mainly used for the transmission part of the circuit so that all high-frequency microwave signals can be transmitted to the load, and almost no signal is reflected back to the source, thereby improving the energy efficiency. It can be seen from the output of the driving circuit that the impedance matching network plays a role in modifying the input impedance of the load system. Impedance matching is done to change the

amount of power delivered to the load.

The condition for impedance matching in this experiment is that the conjugate value of the load impedance and the output impedance of the signal source should be equal. The sum of their modes and angles must be zero so that the maximum power output can be obtained on the load. The topology circuit of only one inductor and one capacitor can be used as the impedance matching network. Because the implementation can be simple, an L matching circuit is used after the LIPUS driving circuit in this experiment. The L-matched impedance transformation network is shown in Figure 2.7.

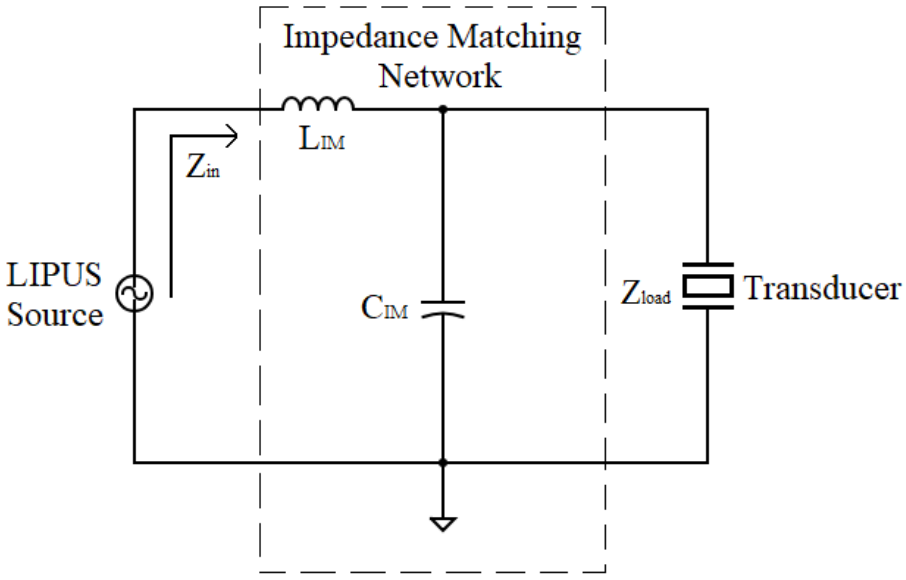

Figure 2.7: L-match circuit for impedance transformation

It is undesirable to drive a reactive load, which causes low network efficiency and a large amount of signal reflection. Impedance matching is to design a circuit to find a match between the power source and the electrical load, which serves to improve the power factor of the power grid by maximizing the network efficiency and minimizing the signal reflection. We adjust the load impedance value by a series and parallel connection of capacitors, inductors, and load to achieve source and load impedance matching. An L-match circuit for impedance transformation was one of the circuits

used to match the impedance between a source and a transducer, as shown in Figure 2.7. We will use this circuit to implement the impedance matching afterward.

Since the impedance transformation network will generate a gain of magnitude n to the signal source, the source only needs to generate a voltage with amplitude $\frac{V_{load}}{n}$ to generate a sinusoidal signal with amplitude V_{load}. Therefore, by derivation, in order to achieve a $1:n$ transformation ratio, the impedance transformation network must reduce the load resistance by n^2 times, which means:

$$Z_{in} = \frac{R_{eq}}{n^2} \tag{2.4}$$

where n denotes the voltage gain achieve by the impedance matching network. Then, we can consider the circuit implementation of the impedance matching network.

As we derived in Appendix A, the input complex impedance Z_{in} can be denoted by the impedance matching components and transducer equivalent impedance:

$$Z_{in} = \frac{R_{eq}}{1+\omega^2(C_{IM}+C_{eq})^2R_{eq}^2} + j\omega\frac{L_{IM} - R_{eq}^2(C_{IM}+C_{eq})(1-\omega^2 L_{IM}(C_{IM}+C_{eq}))}{1+\omega^2(C_{IM}+C_{eq})^2R_{eq}^2} \tag{2.5}$$

where C_{IM} and L_{IM} are the impedance matching capacitor and inductor, respectively. C_{eq} and R_{eq} are the equivalent resistance and capacitor of the ultrasound transducer. $\omega = 2\pi f$ is the resonance angular frequency where $f = 1,500,000$ Hz. The imaginary part of Z_{in} should be set to zero because we would like the input impedance to be a purely resistive load. Therefore, we get the following equation:

$$L_{IM} - R_{eq}^2(C_{IM}+C_{eq})(1-\omega^2 L_{IM}(C_{IM}+C_{eq})) = 0 \tag{2.6}$$

After the derivation, the impedance matching inductor L_{IM} and capacitor C_{IM} are equal to:

$$L_{IM} = \frac{R_{eq}^2(C_{IM}+C_{eq})}{1+\omega^2(C_{IM}+C_{eq})^2R_{eq}^2} \tag{2.7}$$

Then, because the imaginary part of the complex impedance is set to zero, the impedance Z_{in} is updated to be:

$$Z_{in} = \frac{R_{eq}}{1 + \omega^2 (C_{IM} + C_{eq})^2 R_{eq}^2} \tag{2.8}$$

Substitute equation 2.4 to the above equation we will have the expression:

$$C_{IM} = \frac{1}{\omega R_{eq}} \sqrt{n^2 - 1} - C_{eq} \tag{2.9}$$

For different gain values, we will have different impedance matching networks, as shown in Table 2.3.

Table 2.3: Possible impedance matching network values.

Voltage Gain	C_{eq} + C_{LM} **(nF)**	**Capacitor** C_{IM} **(nF)**	**Inductor** L_{IM} (μH)
2	4.177	-	2.022
3	6.821	0.021	1.467
$\sqrt{10}$	7.234	0.434	1.401
4	9.339	2.539	1.130

In order to effectively design the power output stage of the system, it is necessary to specify the sound power requirements of the emitted LIPUS signal. The effective area A of the transducer used in the experiment is 4.91 square centimeters, and the goal of the transducer is to provide a minimum average intensity $I_{SATA} = 6.1 mW/cm^2$, then the transducer needs to provide a minimum average power P_{SATA} of 30 mW because $P_{SATA} = I_{SATA} \times A$. Because the designed LIPUS signal has a duty cycle of 20%, the sound power P in the non-pulsed ultrasound signal must be equal to five times the average power, that is, 150 mW. Therefore, we would like to choose a smaller voltage gain value.

Based on the results calculated in Table 2.3, we can see that if the voltage gain is lower than 3, the sum of C_{eq} and C_{IM} will even be smaller than the capacitance value of C_{eq}, which is 6.8 nF. For the convenience of design, the final L-matching network

for the ultrasound transducer uses a voltage gain that approximately equals to $\sqrt{10}$. The inductance value is 1.4 μH and the capacitance value is $440pF$.

2.3.2 Signal Generator Network

The design goal of the drive circuit is to generate a pulse modulation signal with sufficient energy and adjustable amplitude to drive the piezoelectric transducer through the impedance transformation network designed in Subsection 2.3.1. The Bluetooth module to be discussed in the next section will provide the target signal frequency and pulse duty cycle required by the circuit. The impedance matching network and drive circuit will be implemented on different circuit boards. Because the inductance and capacitance of the impedance matching circuit are relatively large, it will be integrated into the head-mounted therapy device. The driving circuit and the Bluetooth communication circuit will be integrated on a circuit board.

The required signal specifications of two-channel LIPUS generator device are: adjustable intensity of 30 mW/cm^2 to 102 mW/cm^2, 1.5 MHz frequency with pulse repetition rate of 1 kHz and 20% duty cycle. A proposed module diagram is shown in Figure 2.8 to achieve above design.

From the diagram, we can sort out the flow chart of this LIPUS generator module. The Bluetooth module BC113 chip sends the LIPUS prescription to the microcontroller, which contains the treatment duration and intensity. Then the microprocessor will generate a 1-kHz square wave on a pin according to the treatment time. The 1kHz square wave generated by the microcontroller will be superimposed with the 1.5-MHz square wave generated by the crystal through the AND gate, which obtains the modulated LIPUS signal with 5V amplitude, 1.5-MHz frequency, 1-kHz repetition rate with 20% duty cycle.

At the same time, another pin from the microcontroller will set the digital potentiometer to the desired resistance value. The voltage divided on the digital potentiometer will amplify the modulated LIPUS signal through the voltage amplifier.

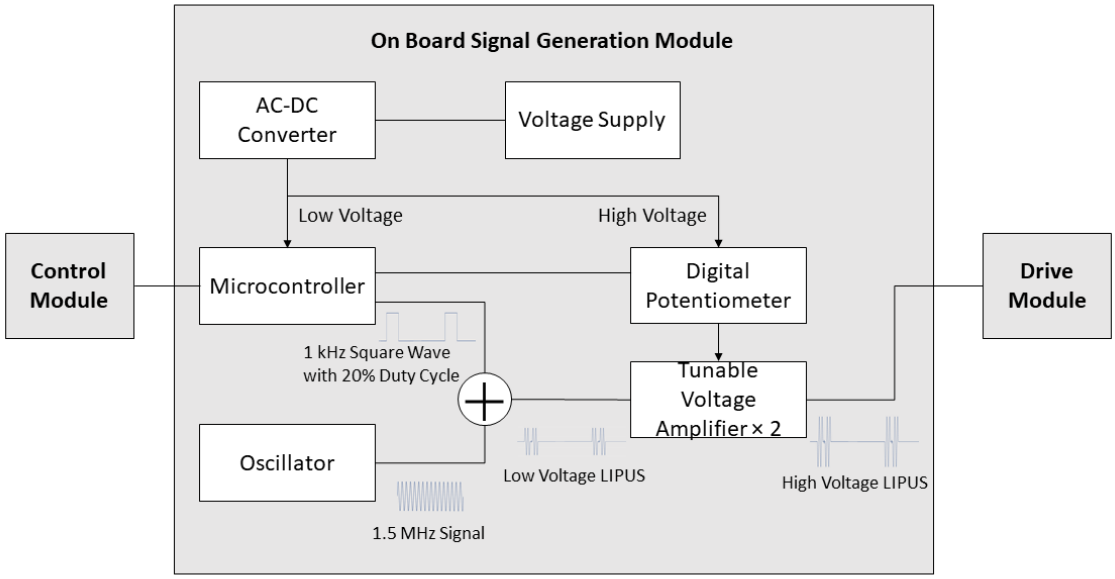

Figure 2.8: Diagram of the signal generator network.

This signal will then be sent to the drive module.

Figure 2.9 provides a LIPUS signal schematic. This signal includes two complete repetition periods (200 microseconds). Among them, each repetitive envelope contains 300 rectangular pulses, which each pulse has a period of $\frac{1}{1.5}$ microseconds. The peak-to-peak amplitude of the signal pulse is 2V. For the fabricated LIPUS generator, a method of controlling the signal's constant, pulse strength will be provided, allowing control of the signal's duration and amplitude.

2.3.3 Bluetooth Control Network

The design concept of the Bluetooth control module is to use the short-range, low-power method to accurately transmit the instructions on the mobile phone to the LIPUS generator. We use BC118 Bluetooth® low-energy module by BlueCreation Inc. to implement the design.

After programming, the BC118 can receive and send data through the UART at 9600 bps. Users can use the module to initiate two types of operations: commands

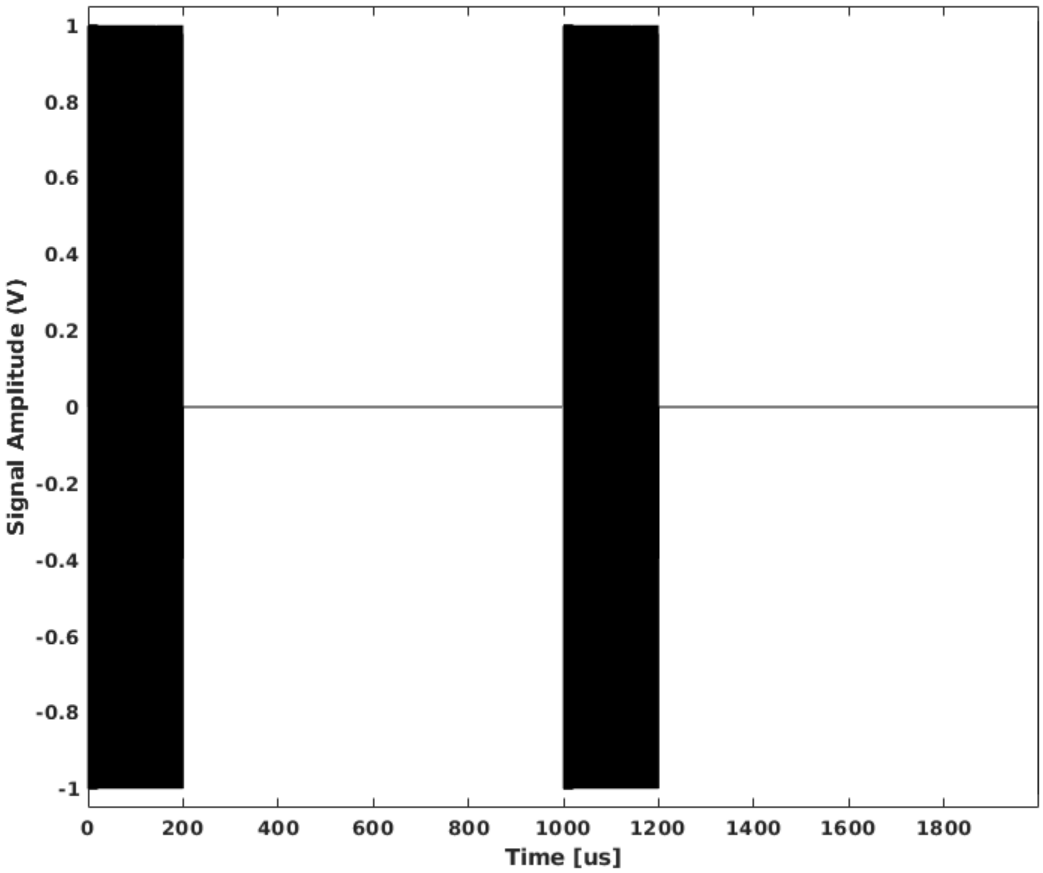

Figure 2.9: Modulated LIPUS signal diagram. Frequency: 1.5 MHz; amplitude: 1 V; repetition rate: 1 kHz; duty cycle: 20%.

and set / get parameters. In this application, we only use the BC118 to transmit commands and do not need to receive data.

The BC118 and the sender (mobile phone) will transfer the data to the microcontroller in the form of a character string. The beginning of the string will use "RCV=" by default, and the end will use the carriage return "\r" by default. For example, if the microcontroller gets the following string: "RCV = 180000.75\n\r". It means that the duration time is 180000 milliseconds, the corresponding voltage signal transmitted to the digital potentiometer is $5 \times \frac{75}{255}$ Volt.

The software is designed based on the Sierra Wireless open-source software (MelodySmart sample application on the Android platform). It can be installed on any Android

phone with a system-level higher than Android 4.3 and communicate with a BC118 Bluetooth chip via UART communication. Compared with the sample application, we modified the user interface to serve the patients better. This application will be developed as an Internet of Things device to allow clinicians to monitor their patients remotely.

Patients/psychiatrist can control the intensity of the LIPUS signal and the duration time of the treatment cycle. Although changing the pulse repetition rate and duty cycle via Bluetooth can be easily achieved, we do not want the clinicians or patients to have such permission. The pulse repetition rate and duty cycle we decide right now (1 kHz with 20% duty cycle) have been demonstrated to be the optimal pair of parameters for treating disease including bone healing, tooth root resorption, inflammation inhibiting, and neuromodulation by many researchers.

Chapter 3

Design of the Headphone for the Wearable Transcranial Low-intensity Pulsed Ultrasound Device

3.1 Background

By collaborating with Dr. Xinmin Li's group at the Department of Psychiatry at University of Alberta, Guo *et al.* discovered that LIPUS could help alleviate depression based on the in-vitro and animal studies [72]. The unfocused planar acoustic waves stimulate neuron cells and made mice happier based on the behavior tests. For future clinical trial usage, we need to design a portable LIPUS therapeutic interface for the TUS application like the one shown in Figure 2.1.

This portable feature allows patients to receive treatment anyplace and anytime. Furthermore, it can become an Internet-of-Things (IoT) device in which the psychiatrists can monitor the treatment via the Internet. A customized application (a mobile App) installed on smartphones in Figure 2.1 enables psychiatrists to remotely prescribe and control ultrasound dosage (intensity and duration) via the combination of Wi-Fi and Bluetooth. The ultrasound generator can drive the transducer using a pulsed square signal generated from the impedance matching board. By embedding transducers and transducer caps inside the headband, patients can simply place the

LIPUS headband for the treatment via the left and the right temples. The ultrasound wave can transmit through the skull and excite the neurons in the hippocampus.

Commonly used ultrasound transducers have a metal cap on top of the piezoelectric crystal to prevent the electrodes from exposed directly to fluids or to the body. Researchers have also investigated the influence of the flexural modes of piezoelectrically actuated metal caps on the beam widths and frequencies [82]. However, as ultrasound is generated from the piezoelectric crystal, it is not suitable to use metal housing caps to touch the facial regions, especially for temple area where is a juncture where the frontal, parietal, temporal, and sphenoid bones fuse together. In addition, it is hygienic and unsafe to use the same aluminum cap or steel cap ultrasound transducer to contact different patients during the therapy directly. Currently, no specific ultrasound transducer cap exists on the market aimed at treatment via the temple area. In this chapter, we design a replaceable rubber cap for the ultrasound transducer and a headphone appearance for the neurostimulation application .

3.2 Ultrasound Transducer Cap Design and Headphone

3.2.1 Acoustic Impedance, Sound Pressure, and Sound Intensity

Part of the medium that is affected by the ultrasonic vibration or space which is full of ultrasound is called the ultrasound field. The physical quantities that characterize the ultrasound field are mainly sound pressure, acoustic impedance, and sound intensity.

Sound pressure is the difference between the instantaneous pressure at a point in the presence of a sound wave and the static pressure of the medium, denoted by P, which is defined by

$$P_{Total} = P + P_{Stat} \tag{3.1}$$

where P_{Total} is the total pressure, and P_{Stat} is the static pressure. The ratio of the

sound pressure P at a certain point of the medium to the vibration particle velocity V at this point is called the acoustic impedance, which is usually represented by Z. Based on the definition, acoustic impedance Z can be obtained by the following equation:

$$Z = \frac{P}{V} = \frac{\rho c A \omega}{A \omega} = \rho c \tag{3.2}$$

where A and ω are the amplitude and angular velocity of the particle vibration, respectively. Acoustic impedance is numerically equal to the product of the density ρ of the medium and the speed of sound c in the medium in $g/cm^2 \cdot s$, with different acoustic impedance for a different medium.

Sound intensity, also known as acoustic intensity, is defined as the power carried by sound waves per unit area in a direction perpendicular to that area.

$$I = Pv = \frac{1}{2}\rho c A^2 \omega^2 = \frac{1}{2}\rho c v^2 = \frac{P^2}{2Z} \tag{3.3}$$

From the Equation 3.3, we can see that the sound intensity is proportional to the square of the sound pressure and proportional to the square of the frequency in the ultrasound field.

Because of our design, we should only consider the reflection and transmission of ultrasound perpendicular to the flat interface. As shown in Figure 3.1, a longitudinal sound wave perpendicular is incident on the interface between two medium.

Notice that at the junction of two mediums, the velocity and pressure in the medium must be balanced at the interface. That is, the incident sound pressure plus the reflected sound pressure is equal to the transmitted sound pressure. On the other hand, the sum of the reflected sound velocity and the transmitted sound velocity is equal to the incident sound velocity. These balance equations can be expressed in terms of pressure and acoustic impedance:

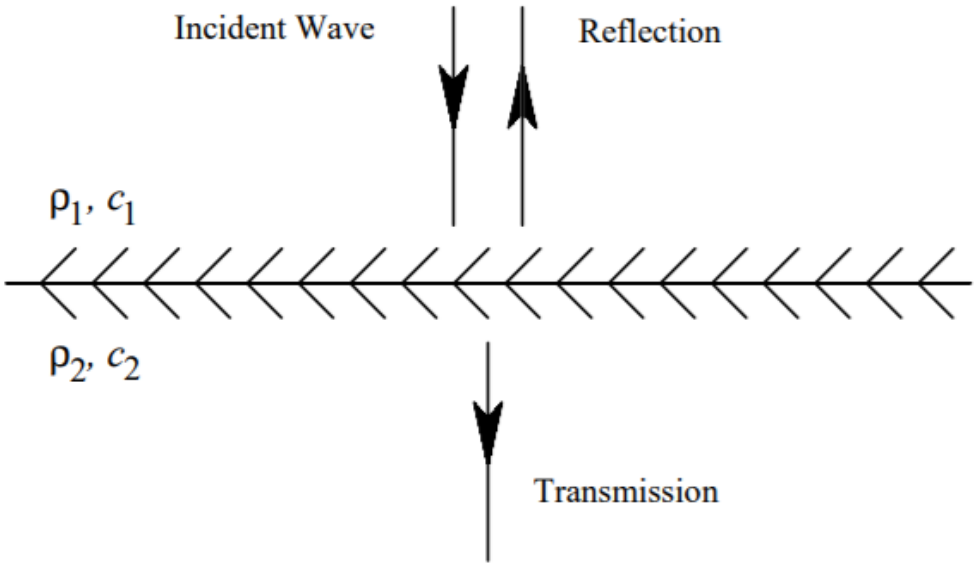

Figure 3.1: Diagram showing an ultrasound wave incident to the interface.

$$\begin{cases} P_i + P_r = & P_t \\ \frac{P_i}{Z_1} - \frac{P_r}{Z_1} = & \frac{P_t}{Z_2} \end{cases} \tag{3.4}$$

where the subscript "i" denotes incident, "r" denotes reflection, and "t" denotes transmission. Z_1 and Z_2 denoted the acoustic impedance of two medium individually. $Z_1 = \rho_1 c_1$, and $Z_2 = \rho_2 c_2$. When the ultrasonic wave perpendicular to a sufficiently large smooth flat interface, the ratio of interface transmission wave pressure P_t to the incident wave pressure P_i is called the transmission coefficient of sound pressure, denoted by t. By deriving Equation 3.4, we can obtain the transmission coefficient of sound pressure as:

$$t = \frac{P_t}{P_i} = \frac{2Z_2}{Z_2 + Z_1} \tag{3.5}$$

Similarly, the ratio of the interface transmission wave intensity I_t to the incident wave intensity I_0 is called the transmission coefficient of sound intensity, denoted by T:

$$
\begin{aligned}
T = \frac{I_t}{I_i} &= \frac{\frac{P_t^2}{2Z_2}}{\frac{P_i^2}{2Z_2}} \\
&= \frac{4Z_1Z_2}{(Z_1+Z_2)^2}
\end{aligned}
\tag{3.6}
$$

Based on Equation 3.6, we can see that when the acoustic impedance of the incident wave and transmission wave medium (Z_1 and Z_2) is equal or similar, the sound intensity of transmission coefficient is close to 1. On the other hand, the greater the acoustic impedance mismatch, the greater the percentage of energy that will be reflected at the interface between one medium and another.

3.2.2 Ultrasound Cap Design

The main job of the coupling agents is to facilitate the transmission of ultrasonic energy from the transducer into the medium. Common coupling media include water, various oils, creams, and gels. Under ideal circumstances, this transmission process will not absorb ultrasonic energy, and its transmission path will not change, so the transmission efficiency is maximized. However, based on the derivation above, this "ideal" is almost impossible to achieve because all media (tissues) have different acoustic impedance characteristics and attenuate the propagation of sound waves. In order to maximize the energy transfer from one medium to another, the impedance of both media must be as similar as possible. Obviously, this is not achievable because ultrasound waves are transmitted from the generator to the tissue and then through different tissue types. The more significant the impedance difference at the boundary, the higher the reflection that will occur, and therefore the less energy will be transmitted.

In addition, there is a small air gap between the transducer and the skin interface. When the ultrasonic signal encounters the steel-air interface, the proportion of reflected ultrasonic waves will approach 99.998% based on Equation 3.6, which means that ultrasonic energy will not be transmitted [83]. Ideally, the coupling medium

should be fluid in order to fill all available space. It should also be relatively viscous, so that it remains in place. It should also have an impedance suitable for the connected medium, and should allow minimal absorption, attenuation or interference of ultrasonic waves.

One of the most significant challenges in the development of the portable LIPUS system is to design an interface that transmits the ultrasound wave gently without causing any thermal damage and mechanical injury to the skin. As we discussed in Section 2 and Figure 2.2, the fabricated ultrasound transducers we used in this research have cylinder aluminum caps at the outside to protect the piezoelectric crystal and other components. It is not preferable to expose the facial regions to a vibrating aluminum cylinder in neither a psychological nor a physiological way.

In our published paper [79], we demonstrated that a polyurethane rubber cap filling with ultrasonic coupling agents could be used as additional transmission media outside the metal cap. In addition, we designed a headphone-style LIPUS transmitting interface that patients can wear them on the head to receive treatment. We will discuss the detailed design in the following content.

The acoustic transmission material can be either solid or fluid. The ideal sound transmission material allows sound waves to pass through to the sound-transmitting layer without any reflections. Therefore, the characteristic acoustic impedance of the material is required to match that of water. The attenuation coefficient of the material should be as small as possible to avoid or alleviate power attenuation during transmission. In this circumstance, we choose polyurethane rubber due to its excellent acoustic characteristic:

- The acoustic impedance Z of polyurethane rubber, the value of ρc (that is, the product of the density of rubber and the propagation velocity of sound waves in rubber) are matched with the ρc value of the sound wave propagation medium, e.g., water [84]. (Acoustic impedance is a property of materials that expresses

how much acoustic pressure is applied to the medium at a corresponding acoustic vibration.)

- The acoustic energy loss is smaller when the sound waves pass through the polyurethane rubber. Garu *et al.* demonstrated that rubber has a relatively low insertion loss and high echo reduction in various frequency ranges [84]. As the temperature increases (from 3.9 °C to 33.6 °C), both sound speed and sound attenuation of the frequency dependence decreases [85].

- Polyurethane rubber is a flexible and ductile material. Using this material as the transducer cap can make the transducer fit tightly to the temple area on the brain. This makes the ultrasonic signal incident as vertical as possible, which reduces the reflection and refraction generated and improves energy utilization. It can enable more ultrasound energy to enter the hippocampus area through the skull.

When acoustic incidents through the polyurethane rubber, the sound attenuation value depends on the rubber composition, which includes two parts: one is the choice of rubber species; the other is the choice of compounding agent.

As shown in Figure 3.2, a plastic base is fixed at the bottom of the transducer. The other side of the plastic is glued with polyurethane rubber, which is formed as a cap with a thickness of 1.6 mm. We build a detachable plastic cap connected with rubber and fixed at the front of the transducer. The transmission cables of the transducer are connected at the back of the piezoelectric crystal, which gives us space to build a separate case for the transducer. A spiral case with a rubber cover was produced.

As we can see in the middle and right figures in Figure 3.2, the male case is stuck securely to the piezoelectric transducer, and the female case is attached with a cylindrical rubber. We first fill the female case shown in the right figure in Figure 3.2 with ultrasound coupling agents and combined with the male case by screwing on the female case, which is presented in the left figure of Figure 3.2. One of the advantages

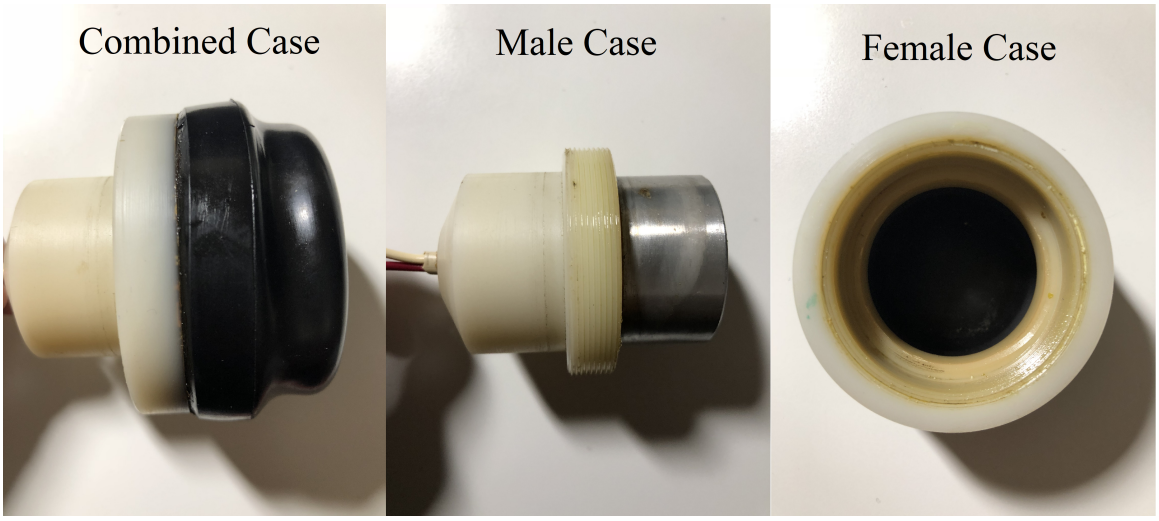

Figure 3.2: Designed transducer cap from three different angles proposed in [79]. Left: the view of combined case; middle: the view of male case and transducer; right: inside view of the female case and rubber.

of this design is that if we fabricate the female case in mass production, the cost of the female case can be affordable for each patient for each LIPUS therapy to prevent cross-infection. The whole ultrasound transducer cap will be hidden in a headband to treat specific areas (e.g., temple), which will be discussed in the remaining section.

3.2.3 Headphone Design

The integrated piece and the individual components of the headband have been presented in Figure 3.3. The headband consists of two impedance transform circuit boards, two ultrasound transducers, two pairs of plastic cases, and two replaceable polyurethane rubber cap filling with the ultrasound agents. The impedance transform circuit board locates inside the male case and connects with a transducer and the input cable. The flat rubber surface in the female case will contact the temple region on the brain, which will be filled with ultrasound agents to provide a better acoustic property for LIPUS signal from the aluminum cap to the polyurethane rubber cap. The male case and female case crew up with each other tightly, which prevents the ultrasound agents from leaking.

Ultrasound is performed by a LIPUS generator device with a piezoelectric trans-

Figure 3.3: Deep look at the design of the headphone for transcranial ultrasound stimulation.

ducer. A small amount of gel is applied to a specific part of the head, and then an ultrasonic transducer with rubber cover is placed over the gel. If there is a significant open wound on the head, other ultrasound methods can be used (ultrasonic gel and acoustic head may promote bacteria to enter or tear the wound). The therapist can change various settings of the LIPUS system to control the duration of the treatment or to change the intensity of the ultrasound using different settings at various stages of rehabilitation.

In Figure 3.4, the LIPUS generator sets the amplitude and duration time of pulsed square wave via the instruction sent by a mobile APP via Bluetooth communication. A piezoelectric transducer which is placed in the headband is driven by pulsed square wave generate LIPUS signal. Impedance matching network allows sufficient power delivery to drive the piezoelectric transducer. Consequently, LIPUS passes through the rubber cap to treat the desired function area of interest in the temple area. The advantages of our wearable LIPUS device are three-fold:

1. This wearable LIPUS device helps patients receive LIPUS treatment conve-

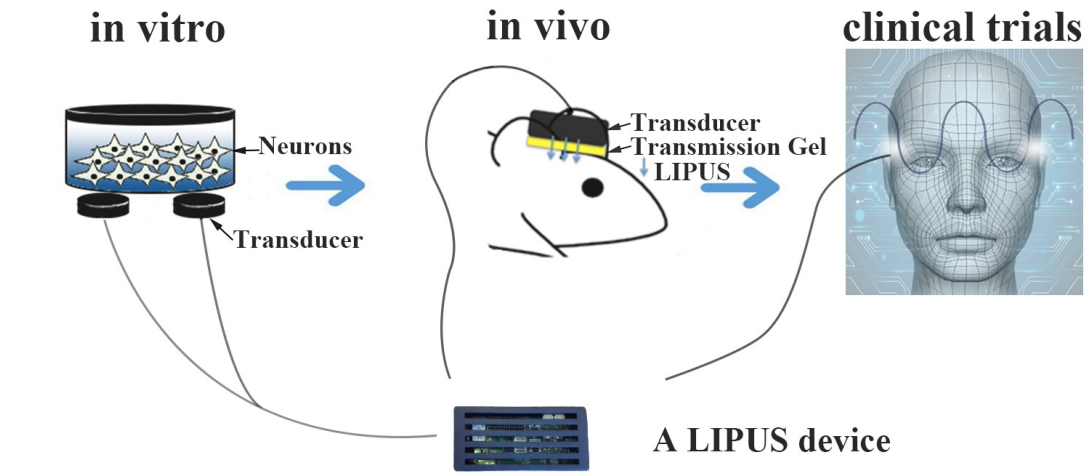

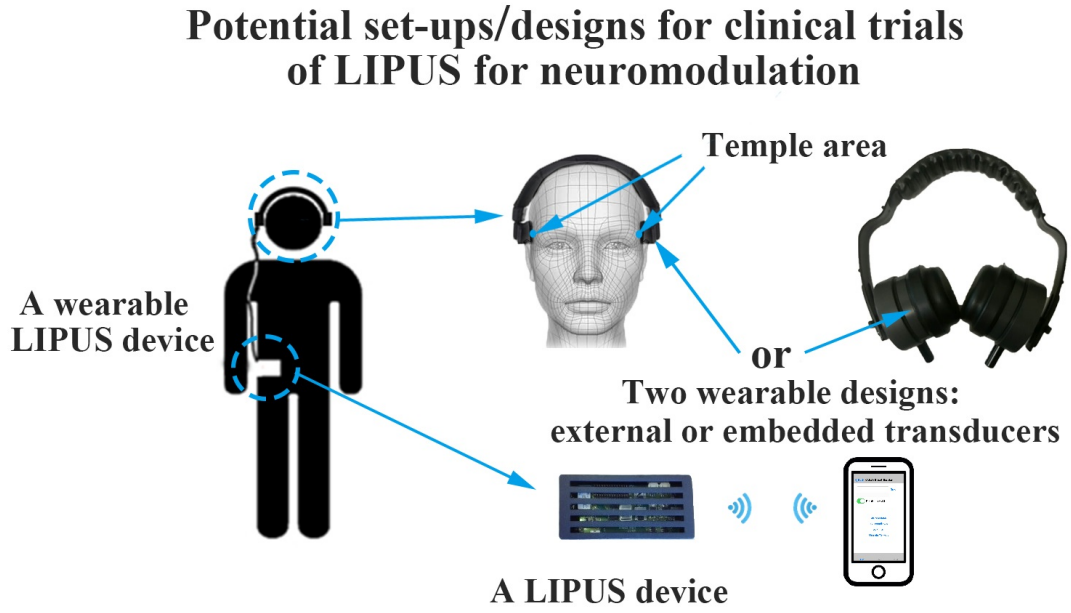

Figure 3.4: Possible LIPUS application in neuromodulation. Upper: the stimulation of the neurons, in-vivo tests on mice, and clinical trials; bottom: the portable LIPUS system designed for TUS application (Modified from [47]).

niently.

2. By using the app on the mobile phone, patients and doctors can remotely control and customize the therapy.

3. Designed transducer cap inside the headband is suitable for mental disease

therapy by decreasing both physical and psychological damage.

3.3 Materials and Experiments

3.3.1 Experiment Equipment and Materials

Four piezoelectric transducers introduced in the previous section are used to conduct the experiment. As we introduced, although the piezoelectric crystal fabricated with transducers should have an exact resonance frequency of 1,500,000 Hz. The real resonance frequency of these transducers is located between 1.5226 MHz to 1.5276 MHz.

Impedance spectroscopy was carried out using an electrochemical measurement station (SP-200, BioLogic Inc., Seyssinet-Pariset, France). At a fixed frequency of 1.5 MHz, four transducers have almost identical impedance spectroscopy of 14.5 Ohm amplitude and negative 70.7-degree phase, which is used to design the impedance matching circuit.

A low-intensity pulsed ultrasound device was designed by the BINARY lab. The output voltage is an amplitude-adjustable 1.5 MHz square wave signal with a 1 kHz repetition rate of 20% duty cycle. The peak-to-peak amplitude varies from 1.25 V to 12.5 V, which is equivalent to LIPUS intensity of around 6 mW/cm^2 to 120 mW/cm^2. Incident wave intensity increases with the increase of output signal amplitude.

Polyurethane rubber is cast into a cylindrical shaped cap and glued at the front of the plastic holder. The rubber was ground to 1.6mm thickness and used to fill the gap between transducer and rubber with three different ultrasound coupling agents (Milli-Q water, transformer oil, and ultrasound gel). The acoustic parameters of three ultrasound agents and polyurethane rubber are presented in Table 3.1.

3.3.2 Experiment Methods

As shown in Figure 3.5, a LIPUS device is used to generate a square waveform of tunable amplitude. The LIPUS device was made in the BINARY LAB at the Univer-

Table 3.1: Acoustic properties of ultrasound agent materials.

	Sound Velocity (mm/s)	**Density** (g/cm^3)	**Acoustic Impedance** $(MRayl)$	**Attenuation Coefficient** (dB/cm)
Water-liquid at 20 °C	1.48	1.00	1.48	-
Oil-transformer*	1.39	0.92	1.28	-
Ultrasound Gel**	1.58	1.02	1.61	0.54 dB/cm at 6 MHz
Polyurethane Rubber	2.09	1.30	2.36	-

* Oil-transformer (100005, Briggs & Stratton Company, Milwaukee, USA)
** Ultrasound Gel (Aquasonic 100, Parker Laboratories, Inc., Fairfield, USA)

Figure 3.5: Photograph of the proposed setup for measuring acoustic impedance.

sity of Alberta, Canada. The output amplitude can be controlled by mobile phone via Bluetooth. The impedance matching board and transducer in the headphone are

disassembled to suit the measurement requirements of the ultrasound power meter. Using the above setup, a set of measurements was performed during which the acoustic intensity generated by the ultrasound transducer was read from an Ultrasound Power Meter (Model UPM-DT-1AV from Ohmic Instruments Co., Maryland). These measurements were performed in the vicinity of the nominal resonance frequency of 1.5 MHz. A plastic holder was placed above the Ultrasound Power Meter. By changing the different transducer caps (no cap/sham group, cap filling with water, cap filling with oil, and cap filling with ultrasound gel) on the plastic holder, we obtained the corresponding intensity at the same driving signal. As the amplitude increases, the intensities of different caps increase, respectively.

After obtaining the acoustic intensity data, we analyzed the attenuation/transmission coefficient (the efficiency of electrical energy into mechanical energy) of each kind of caps using MATLAB. The transmission efficiency was investigated by fitting a linear function between the decayed intensity and the initial intensity.

3.4 Results

3.4.1 Intensity Measurement Result

Figure 3.6 describes the measured ultrasound intensity and fitting intensity of ultrasound transducers with polyurethane rubber filling with different ultrasound coupling agents comparing to the intensity of a transducer without a cap. Three point-data groups (with error bars) are the intensity measurement data for different ultrasound agents compared to the sham group. Each data point represents the average of four measurements, and the standard deviation was calculated to draw the error. The intensity value was obtained by the ultrasound power measured by Ultrasound Power Meter divided by 5 cm^2 effective area of the transducers. Due to the low intensity that we used in the experiment, ultrasound power can be affected by the slight vibration of the table or human movement. However, the overall standard deviation for each

intensity was found to be very insignificant compared to the intensity value.

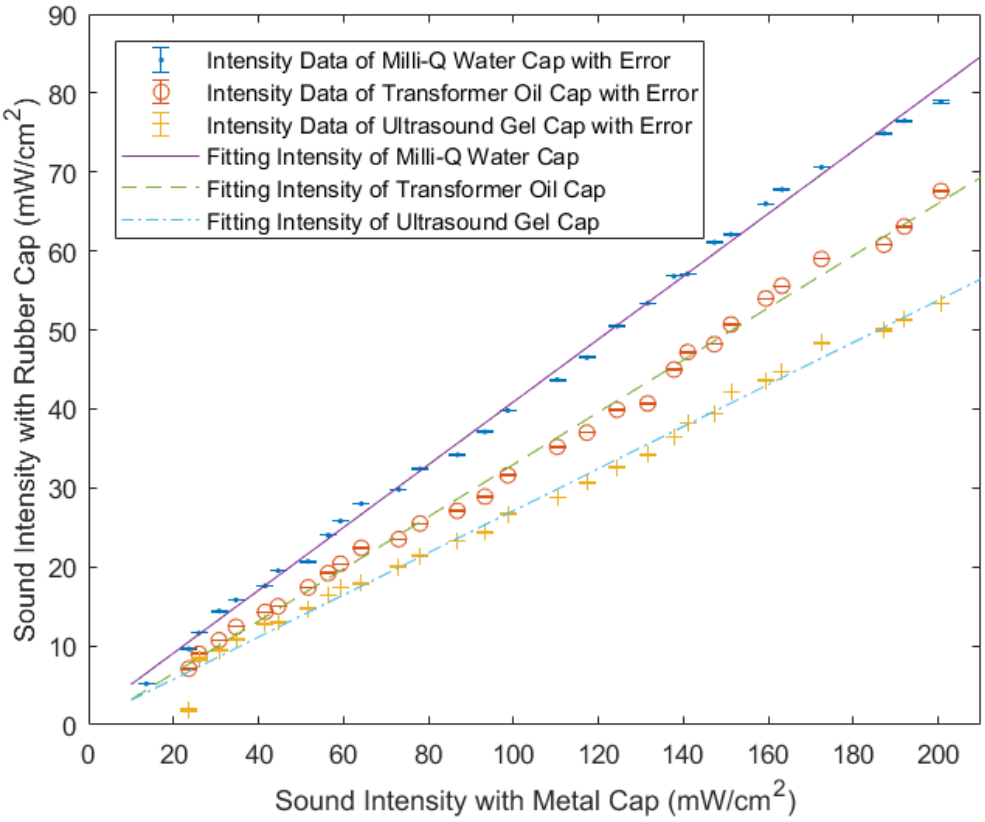

Figure 3.6: Sound intensity measurement and attenuation fitting intensity of sham group and rubber group with different coupling agents.

In order to express the intensity attenuation better, ultrasound intensity attenuation linear fitting was then generated by polynomial curve fitting shown in Figure 3.6 (solid line, dotted line, and dash-dotted line) for each coupling agent. We chose linear fitting because the attenuation of ultrasound intensity is linear based on the data in Figure 3.6. It can easily be seen that rubber cap with Milli-Q water has a higher slope than the other two groups.

3.4.2 Comparison Result of Different Coupling Agents

Comparisons between three different ultrasound coupling agents (Milli-Q water, transformer oil, and ultrasound gel) for intensity attenuation were carried out, as shown

in Figure 3.7. The results return the coefficients for a polynomial of degree 1 (slope) that is the best fit for various data using MATLAB. Insignificant Bias (polynomial of degree 0) was discarded since all the relationships should start at the coordinate origin.

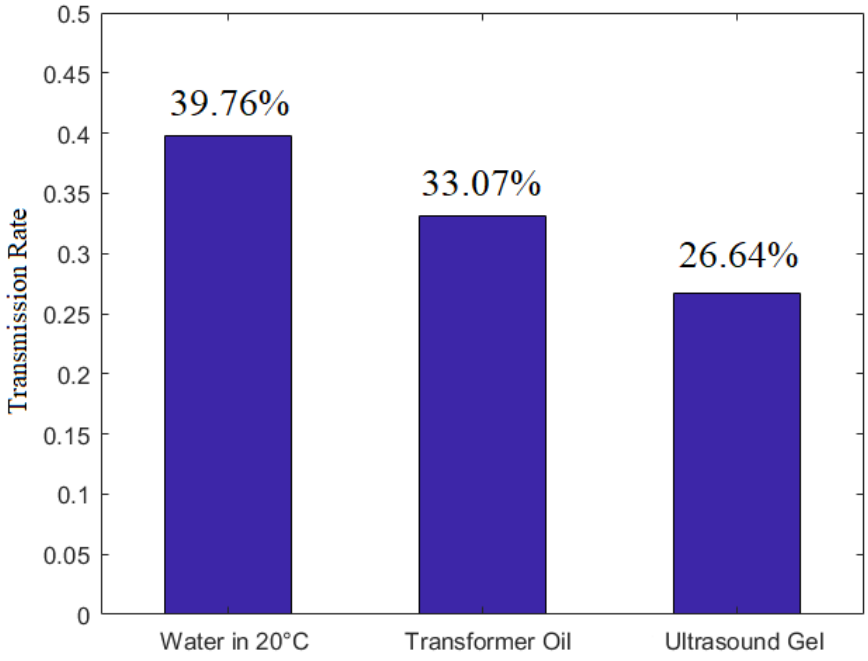

Figure 3.7: Comparison of transmission rates.

Based on the experiment results, polyurethane rubber caps filled with Milli-Q water have significantly higher transmission rates compared to caps filled with oil and ultrasound gel. Theoretically, ultrasound gel has the closest acoustic impedance ρc value to rubber in comparison of the three mediums, which should lead to the best transmission rate based on Equation 3.6. Nonetheless, ultrasound gel has a higher attenuation coefficient that cannot be ignored when ultrasound waves transmit through the ultrasound gel, as shown in Table 3.1. That might be the main reason using ultrasound gel as the filling medium has turned out to be the worst scenario. The coupling agent with the second closest acoustic impedance is Milli-Q water, and its optimal transmission rate is 39.76%.

Chapter 4

Safety Assessment of the Transcranial Low-intensity Pulsed Ultrasound Equipment

As we discussed in Chapter 1, transcranial ultrasound stimulation as a new neuromodulation method is attracting more and more attention from researchers. Many studies have shown the potential therapeutic effect of transcranial LIPUS stimulation on mental disorders. Increasing neuronal activity and regulating BDNF factor levels are some of the beneficial effects of the transcranial LIPUS.

One common side effect of standard transcranial ultrasound stimulation is that the skin and the temple area of the brain are easily overheated due to its thermal effect. Among all the stimulation techniques, a typical example is the high-intensity focused ultrasound (HIFU). Due to its characteristics of focused ultrasound, it is easy to deliver high-intensity ultrasound energy to the focused area. Compared with HIFU, LIPUS has much lower thermal effects due to its unfocused and pulsed ultrasound characteristics. Research conducted by Sun *et al.* demonstrates that LIPUS can reduce the volume rate of tissue heating and reduce the possibility of cavitation [86].

However, some studies have raised different views [72]. In a preliminary study of pulsed ultrasound with an intensity above 100 mW/cm^2, Guo et al. noted that animals receiving LIPUS stimulation suffer from side effects. At an intensity higher than 350 mW/cm^2, the mice will die directly. After LIPUS stimulation with the

intensity of 300 mW/cm^2 for 5 minutes, the mice entered a moribund state. Five minutes LIPUS treatment at an intensity of 250, 200, and 150 mW/cm^2 caused damage to the outer ear of the mice.

In response to these different viewpoints, we hope to analyze the possible side effects of transcranial LIPUS stimulation. In this study, we evaluate the safety of the new portable head-mounted LIPUS treatment system designed in Chapters 2 and 3. Sound pressure simulation and brain temperature simulation are carried out in the computer simulation experiment. In vitro experiments are conducted on the penetration of ultrasound intensity into the skull and skin.

4.1 Material and Methods

4.1.1 Software Stimulation Experiment

The temporal acoustic intensity (I_{TA}) of the ultrasound field generated by the transducer surface is simulated with the k-Wave MATLAB toolbox [87]. The k-wave toolbox is an acoustics toolbox developed by Bradley Treeby *et al.*

The software is designed for time-domain acoustic and ultrasound simulations in complex and tissue-realistic media. The simulation functions are based on the k-space pseudo-spectral method and are both fast and easy to use. It can be used to simulate and reconstruct the photoacoustic wave field. *"The forward simulation is based on the k-space pseudo-spectral time domain solution and couples first-order acoustic equations for homogeneous or heterogeneous media in one, two and three dimensions"* [87].

In the experiment, we use the simulation function of this toolbox, combined with the acoustic characteristics of the objects we need to use, to simulate the distribution of ultrasound acoustic pressure, volume rate, and temperature in the brain.

4.1.2 Transmissibility of Ultrasound Intensity Experiment

In addition to safety assessment, we also need to verify whether this portable LIPUS therapeutic instrument can deliver a sufficiently intense of LIPUS signal to the target area through the skin and skull when it is used for transcranial ultrasound stimulation.

The portable low-intensity pulsed ultrasound device described in the previous chapters is designed and fabricated. The parameters specifications of this portable LIPUS device are listed in Table 2.1. Two ultrasound transducers attached with the portable LIPUS device (longitudinal wave transducers) are fabricated by APC International Ltd., Macheyville, USA. The characteristic of these transducers is introduced in Chapter 2. The set of intensity measurements is performed during which the acoustic intensity generated by the ultrasound transducer is read from an Ultrasound Power Meter (Model UPM-DT-1AV from Ohmic Instruments Co., Maryland).

Human skin and skull structures are simulated by using alternatives. We use chicken skulls to substitute human brain skulls and use chicken skin to substitute human skin. In terms of brain tissue substitutes, we use different substances, all of which have similar acoustic properties to brain tissue. Table 4.1 illustrates the acoustic properties, e.g., density, velocity, of those materials. The detailed properties of the brain, which have been proposed by White *et al.* [88], are listed in the second line of the table. The acoustic properties of those materials shown in the table are proved to be very close when compared to the published properties of the corresponding brain tissues that those materials mimicked [89].

4.2 Experiment Design

4.2.1 Software Stimulation Experiment

When conducting simulation experiments, we need to model the ultrasound signal and the transmission area (that is, the brain). The center of the cylinder transducer surface is located at Y = 0 mm and was perpendicular to the horizontal plane (XZ

Table 4.1: Acoustic properties of brain tissue substitutes.

Material	**Velocity** (m/s)	**Density** (kg/m^3)	**Attenuation** $(dB \cdot cm^{-1} \cdot MHz^{-1})$	**Impedance** $(MRayl)$
Brain [88]	1560	1040	0.6	1.62
Oil Gel-based [89]	1480	1040-1060	0.4-1.8	1.52-1.67
Tofu	1520	1059	0.75	1.48-1.60
Water-based [53]	1480	1000	0.0002	1.48

plane). We used a LIPUS signal with parameters in Table 2.1 as the input source of the brain environment.

The weight of an adult human brain ranges from 1,300 to 1,400 g [90]. Its average width is about 140 mm, the average length is about 167 mm, and the average height is about 93 mm [91]. The average thickness at the center of the pterion is around 4.4 mm which vary individually, making itself known as the weakest part of the skull [92]. Image results indicated that the structure of the human skull is a sandwiched architecture which a layer of trabecular bone is located between two layers of cortical bone [93]. Statistic data showed a significant difference in bone thickness of these three layers from age 20 to 100 years and between male and female [93]. For 20 years old male, the average thickness at the center of the pterion will be estimated as outer cortical bone of 2.3 mm thickness, trabecular bone of 0.4 mm thickness, and inner cortical bone of 1.7 thickness.

We defined a two-dimension Cartesian grid to mimic the horizontal plane of the human brain. The x-axis represents the frontal axis which is parallel to the transmitting direction of the ultrasound wave. The y-axis denotes the Sagittal axis of the human body. In this horizontal plane, we defined the shape of the brain as a rectangle instead of an irregular circle. The reason why we choose to simplify the model is that the transducer we used to deliver the LIPUS is a flat surface transducer and barely ultrasound signal will reach the around bone structure and produce reflection and

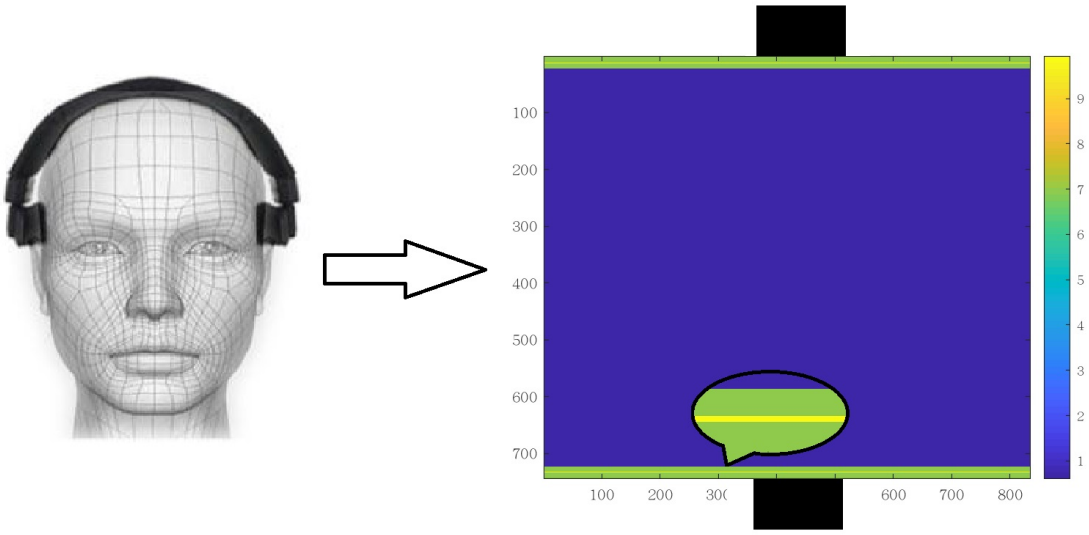

Figure 4.1: Architecture used to mimic a brain.

refraction signals. Figure 4.1 demonstrates a heterogeneous propagation medium we defined to perform the acoustic pressure field and brain temperature simulation.

The grid size (resolution) of the heterogeneous propagation medium is 0.2 mm by 0.2 mm. The medium has 744 (148.8 mm) grid points in the x-direction and 835 grid points in the y-direction (167 mm). In Figure 4.1, the green and yellow sandwich structure represents the thickness of cortical and trabecular bone (inner cortical bone of 9 grid points, trabecular bone of 2 grid points, outer cortical bone of 11 grid points). The colormap of the whole structure denotes the attenuation coefficient of tissues (cortical and trabecular bone, brain). The acoustic properties of the brain tissues are listed in Table 4.2.

The parameters of the LIPUS signal used in the simulation are listed in Table 1. For the SATA intensity delivered by the dual transducers, we chose to use 30 mW/cm^2, 60 mW/cm^2, 90 mW/cm^2, and 120 mW/cm^2 respectively.

The low-intensity pulsed ultrasound system described in the previous section was designed and fabricated in the BINARY lab. The design specifications of this LIPUS treatment system are shown in Table 1. In this paper, a LIPUS signal was applied

Table 4.2: Acoustic and thermal properties of brain tissues.

Material	**Velocity** (m/s)	**Density** (kg/m^3)	**Attenuation** $(dB \cdot cm^{-1} \cdot MHz^{-1})$	**Impedance** $(MRayl)$	**Heat Capacity** $(J \cdot kg^{-1})$	**Thermal Conductivity** $(W \cdot m^{-1} \cdot)$
Bone, Cortical	3476	1975	6.9	7.38	1313	0.32
Bone, Trabecular	1886	1055	9.94	1.45	2274	0.31
Brain	1560	1040	0.6	1.62	3630	0.51

via this ultrasound system, by stimulating the brain mimic environment to assess the safety consideration. The peak rarefactional pressure of the LIPUS at specimen was calculated by the following equation:

$$I_{SATA} = \frac{P_{\text{peak}}}{2\rho c} \tag{4.1}$$

whereas I_{SATA} denotes spatial average and temporal average intensity of the LIPUS signal, ρ denotes the density of specimen and c represents the sound speed at specimen. Based on the Equation 4.1, we can calculated the peak rarefactional pressure of the LIPUS signal that we will be using for the stimulation.

4.2.2 Transmissibility of Ultrasound Intensity Experiment

The experiment setup is shown in Figure 4.2. The wearable LIPUS device transmits ultrasonic waves with difference level intensities (30 mW/cm^2, 60 mW/cm^2, 90 mW/cm^2, and 120 mW/cm^2). As we introduced in the previous section, the average width of an adult human brain is around 140 mm. That means the average length between the ultrasound transducer placed on the pterion area and the center of the brain is around 70 mm. In our experiment, we conduct the in-vitro simulation by the following steps:

- Connect the chicken skin and chicken bones with the ultrasound probe;

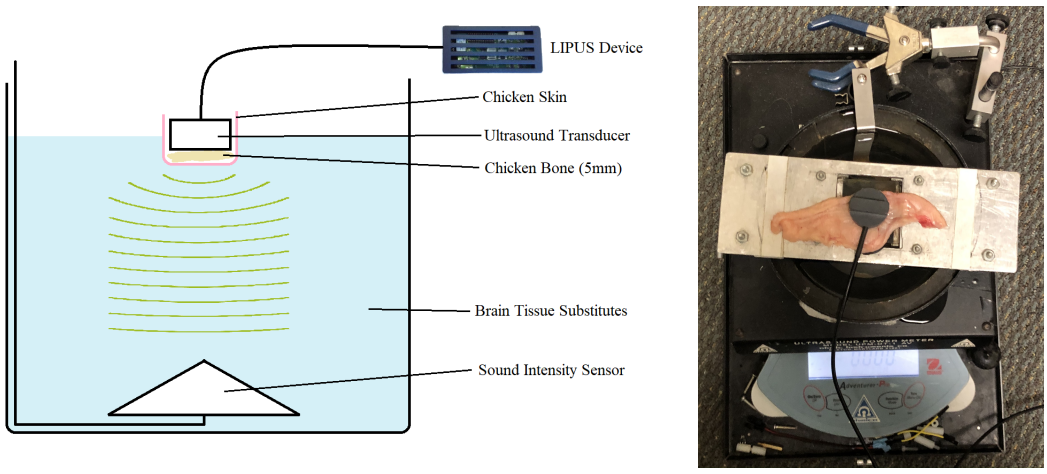

(a) (b)

Figure 4.2: Mimicking the transmission path through skull in the ultrasound power meter. (a) Diagram of the set up; (b) photograph of the set up.

- Fill the ultrasound power meter with brain tissue substitutes, the simulated brain tissue substitutes are introduced in Table II;
- Start the device to emit ultrasound waves, which has four different intensity level;
- Read the intensity displayed at the Ultrasound Power Meter. This intensity value is used to simulate the intensity of ultrasound that can be received in the center of the brain.

Same as in Chapter 3, the detecting intensity is read from an Ultrasound Power Meter (Model UPM-DT-1AV from Ohmic Instruments Co., Maryland).

4.3 Software Simulation Results and Discussion

As shown in Figure 4.3, four groups of color map demonstrate the ultrasound diffusion field simulation results and temperature field simulation results. The reddish color represents higher values (pressure amplitude value, volume rate, and temperature value), while the bluish color represents lower values. In Figure 4.3 (a), it

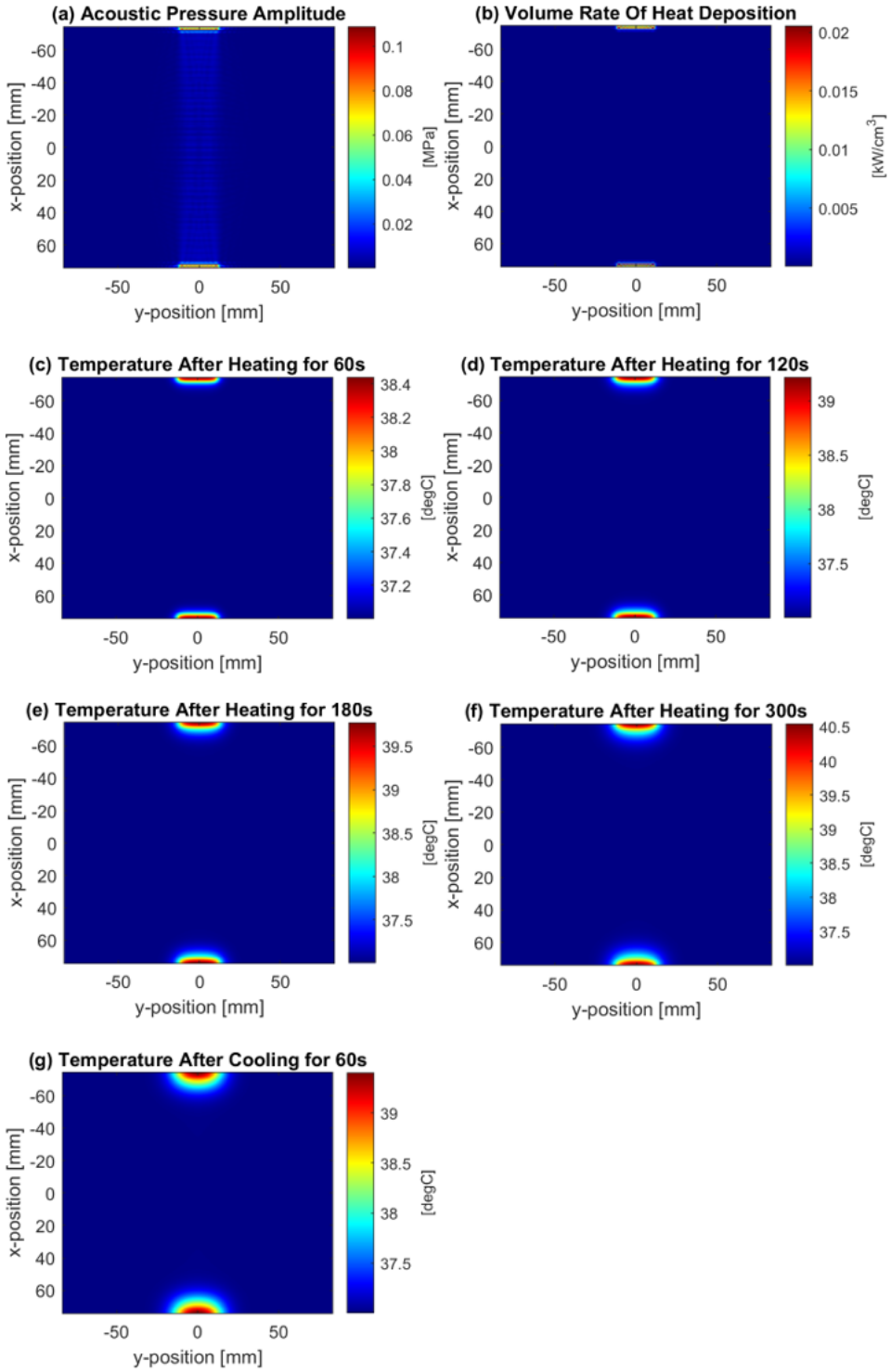

Figure 4.3: Simulation analysis results for 30 mW/cm^2 LIPUS stimulation. (a) Acoustic pressure amplitude; (b) volume rate of heat deposition; (c) temperature after heating for 60 s; (d) temperature after heating for 120 s; (e) temperature after heating for 180 s; (f) temperature after heating for 300 s; (g) temperature after cooling for 60 s.

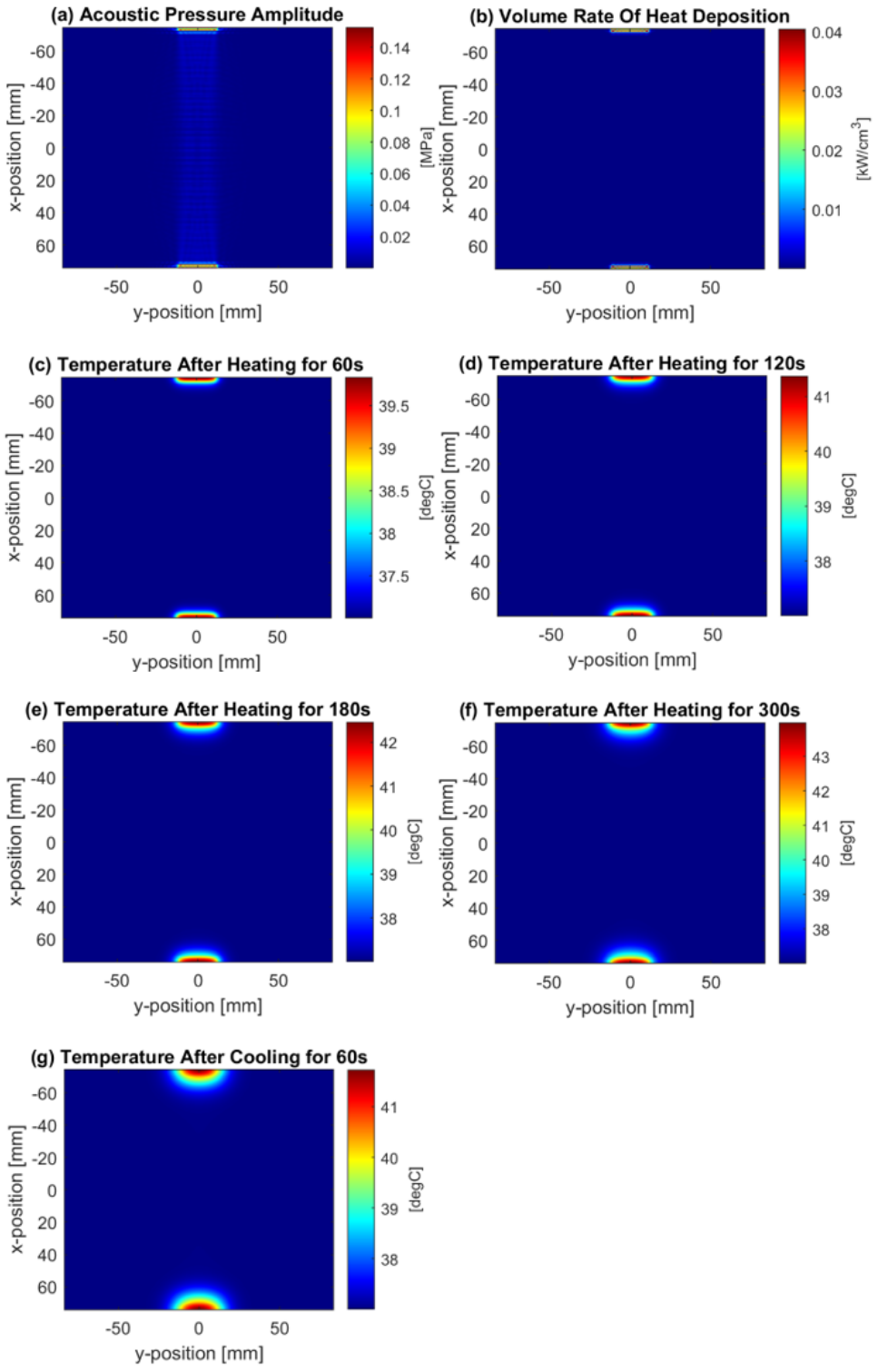

Figure 4.4: Simulation analysis results for 60 mW/cm^2 LIPUS stimulation. (a) Acoustic pressure amplitude; (b) volume rate of heat deposition; (c) temperature after heating for 60 s; (d) temperature after heating for 120 s; (e) temperature after heating for 180 s; (f) temperature after heating for 300 s; (g) temperature after cooling for 60 s.

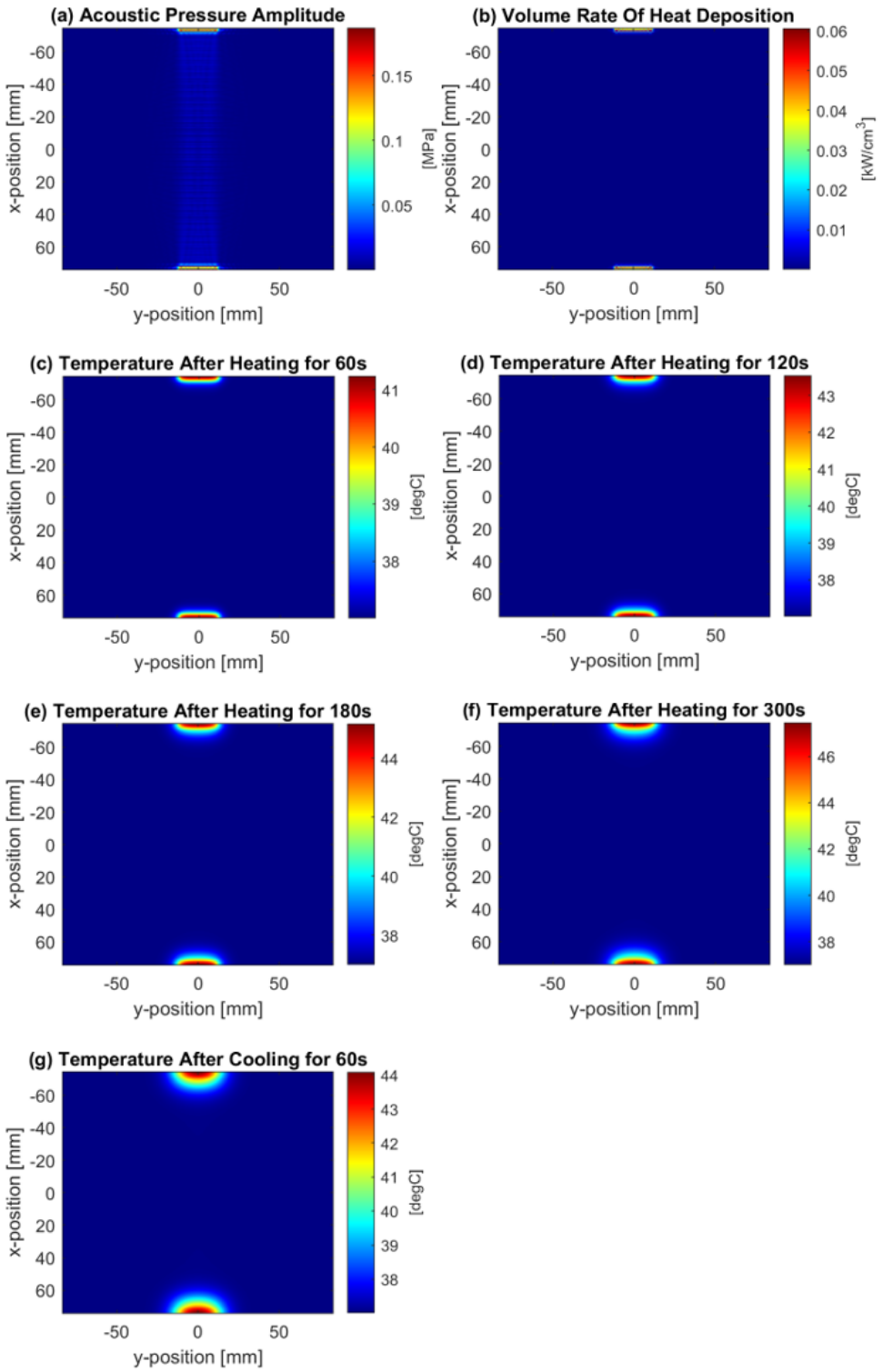

Figure 4.5: Simulation analysis results for 90 mW/cm^2 LIPUS stimulation. (a) Acoustic pressure amplitude; (b) volume rate of heat deposition; (c) temperature after heating for 60 s; (d) temperature after heating for 120 s; (e) temperature after heating for 180 s; (f) temperature after heating for 300 s; (g) temperature after cooling for 60 s.

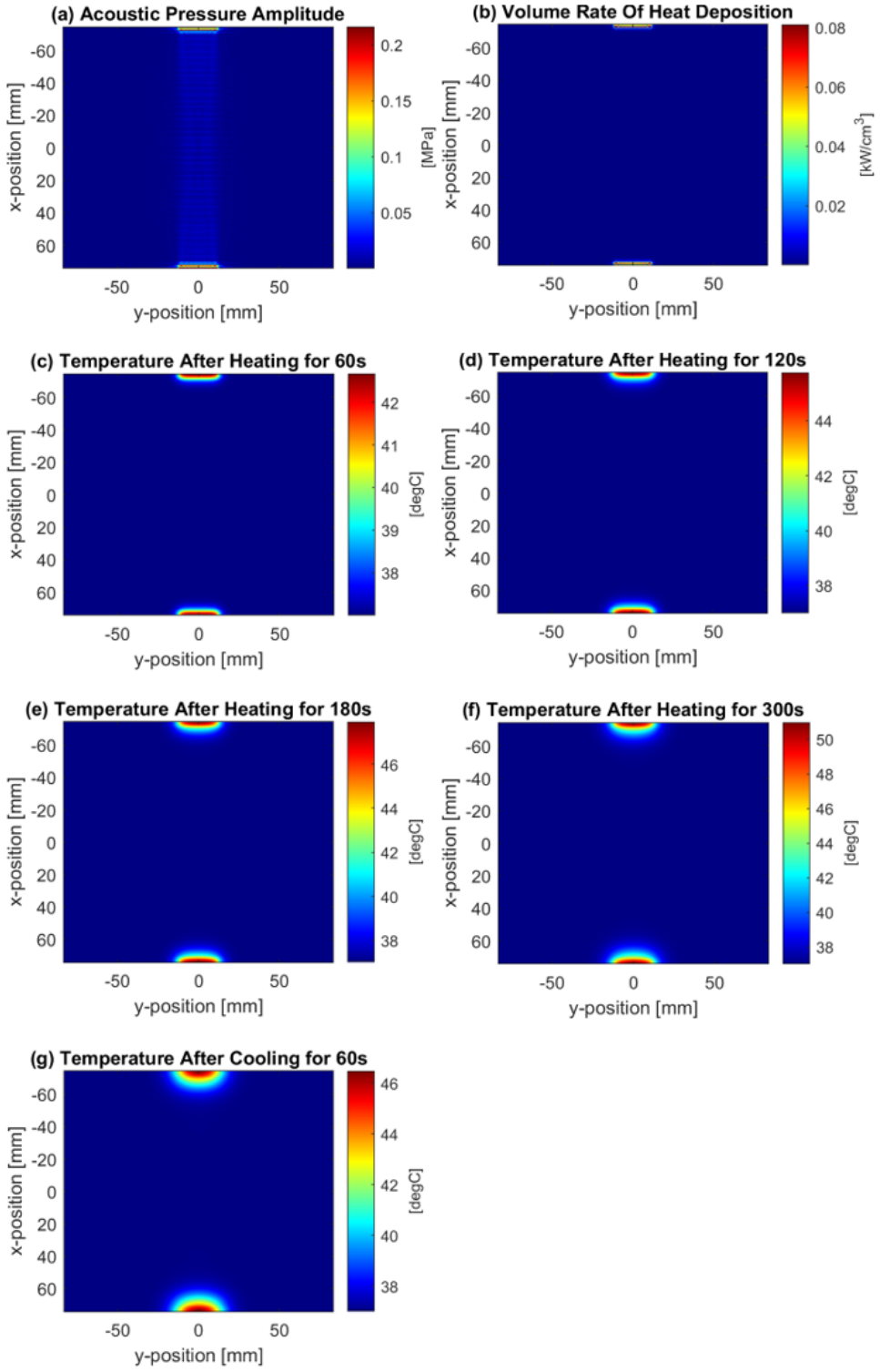

Figure 4.6: Simulation analysis results for 120 mW/cm^2 LIPUS stimulation. (a) Acoustic pressure amplitude; (b) volume rate of heat deposition; (c) temperature after heating for 60 s; (d) temperature after heating for 120 s; (e) temperature after heating for 180 s; (f) temperature after heating for 300 s; (g) temperature after cooling for 60 s.

shows an ultrasound pressure diffusion colormap delivered by 30 mW/cm^2 ultrasound intensity. We can see that the pterion area attached to the transducers has the highest-pressure distribution (red-yellowish area). The middle area of the medium has a mild ultrasound transmission pressure. Ultrasound produces a large amount of reflection when it encounters a heterogeneous interface. The greater the difference in acoustic impedance of the heterointerface, the worse the transmission capability of the ultrasonic wave (the more acoustic reflection it will generate). At the same time, the attenuation coefficient of ultrasound in the sandwich three-layer structure bone is high, and only a small amount of sound intensity can transmit through the bone to reach the brain. After the simulation, the peak sound pressure amplitude reaching the center of the brain is about 5,058 Pa, equivalent to 2.81 mW/cm^2 of sound intensity.

The second to the seventh figures in Figure 4.3 represent the results of the thermal simulation. The second figure in Figure 4.3 (a) calculates the volume rate of heat deposition of the heterogeneous medium. A huge amount of heat volume is generated from the center area of bone which is attached to the transducers. Rest of the bone area and brain area, however, produces almost no heat. The third to the sixth figures represent the temperature distribution after heating for 60 s, 120 s, 180 s, and 300 s, respectively. The maximum temperatures of the entire medium are 38.4 degrees Celsius, 39.2 degrees Celsius, 39.8 degrees Celsius, and 40.5 degrees Celsius, respectively. In addition, the temperature colormap of 300 s treatment followed by a 60 s cooling time is conducted, which has a maximum temperature of 39.4 °C. From all the temperature diffusion color maps, the rise in temperature mainly occurs in the bone areas which are attached to the transducers. The center of the brain has no significant temperature rise.

The other three simulation results with different ultrasound intensity have the same trend as Figure 4.3. In Figure 4.4, the stimulated ultrasound intensity has increased to 60 mW/cm^2. The peak sound pressure amplitude of the center of the brain is

about 7,315 Pa, which is equivalent to 4.06 mW/cm^2. The maximum temperatures after four different treatment duration time and 60 s cooling time are 39.8 degrees Celsius, 41.4 degrees Celsius, 42.5 degrees Celsius, 44.0 degrees Celsius, and 41.7 degrees Celsius, respectively.

In Figure 4.5, the stimulated ultrasound intensity has increased to 90 mW/cm^2. The peak sound pressure amplitude of the center of the brain is about 11,214 Pa, which is equivalent to 6.23 mW/cm^2. The maximum temperatures after four different treatment duration time and 60 s cooling time are 41.2 °C, 43.5 °C, 45.2 °C, 47.4 °C, and 44.1 °C, respectively.

In Figure 4.6, the stimulated ultrasound intensity has increased to 120 mW/cm^2. The peak sound pressure amplitude of the center of the brain is about 12,984 Pa, which is equivalent to 7.21 mW/cm^2. The maximum temperatures after four different treatment duration time and 60 s cooling time are 42.7 °C, 45.8 °C, 47.9 °C, 51.0 °C, and 46.5 °C, respectively.

In addition, we can find from the simulation results that the place with the highest volume ratio is located at the temple where the ultrasonic transducer is placed. In most brain areas inside the skull, there is no obvious volume rate or temperature rise. This is because when ultrasonic waves pass through the skull of the sandwich structure, a large amount of reflection and refraction will produce at the interface of the trabecular bone and the cortical bone. In addition, due to the sparse and porous trabecular bone, a large amount of ultrasound energy will be consumed here.

4.4 Transmissibility of Ultrasound Intensity Experiment Results

The sound intensity level of the LIPUS transmissibility has been carried out, as shown in Figure 4.7. The results return that the sound intensity level decreased by transmitting through the chicken bone and skin. Error bars are calculated from 10 times of measurement for each brain tissue substitutes.

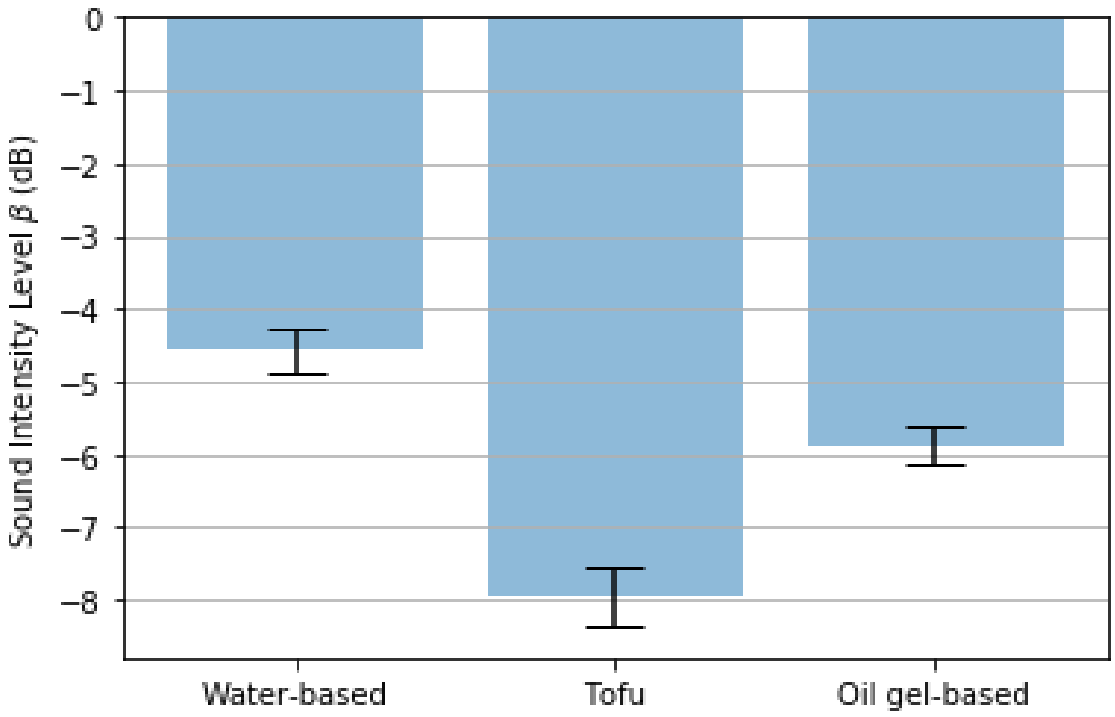

Figure 4.7: Sound intensity level of three brain substitutes.

Because of the lowest sound attenuation coefficient, the water-based brain tissue substitute has the highest sound intensity level of -4.6 dB. The tofu-based brain tissue substitute, with the highest sound attenuation coefficient among the three materials, has the lowest sound intensity level of -8.0 dB. The results comparable to computer simulations validate the feasibility of using ultrasound to stimulate the brain through the skull to relieve mental illness symptoms.

4.5 Discussion

Based on the ASTM C1055 guide (the Standard Guide for Heated System Surface Conditions that Produce Contact Burn Injuries), when the skin is exposed to temperatures greater than 36 degrees Celsius, humans will begin to feel warm. When the temperature is greater than 40 degrees, it will start to feel hot. When the temperature is between 44 degrees and 52 degrees, the skin starts to appear slightly red, with mild pain near the threshold. When the temperature rises above 52 degrees to

60 degrees, the pain increases, and the redness of the skin deepens. The intake at this time is completely reversible. When the temperature is greater than 60 degrees Celsius, people will become numb, and the skin will become red and white alternately, at this time, the skin may have irreversible damage. Objects higher than 72 degrees in direct contact with the skin will cause irreversible damage. The contact refers to the long time contact between the skin to the object. The detail of the ASTM C1055 guideline is concluded in Table 4.3

Table 4.3: Temperature limits for skin contact with the surfaces [94].

Temperature Range (Degree Celsius)	**Sensation**	**Skin Color**	**Injury**
Below 33	Cold	-	None
33 - 40	Warm	Flushed	None
40 - 44	Hot	Flushed	None
44 - 52	Threshold Pain	Light Red	Reversible
52 - 60	Severe Pain	Bright Red	Reversible
60 - 72	Numbness	Mottled Red and White	Possibly Reversible
Higher than 72	Numbness	White	Irreversible

According to computer simulation results, when using a higher intensity of 120 mW/cm^2 LIPUS stimulation, the accumulated temperature at the skin will reach 51 degrees Celsius after five minutes. At this temperature, people will feel a little tingling, and the skin will cause reversible damage. When we use a lower intensity (30 mW/cm^2 or 60 mW/cm^2) LIPUS signal, stimulation for five minutes will only cause the skin surface to produce a maximum temperature of 44 degrees Celsius. At this temperature range, the skin will not cause any damage, and people will not feel any discomfort.

On the other hand, according to the LIPUS intensity penetration test, if we use the

60 mW/cm^2 LIPUS signal as the stimulation source, the LIPUS intensity that can be received in the brain is range from 23 mW/cm^2 to 35 mW/cm^2. We can conclude that the transcranial LIPUS stimulation can transmit enough energy through the skin and skull to the brain without causing significant thermal damage.

Chapter 5

Conclusion and Future Work

Mental disorders have become a significant problem in the world. Low-intensity pulsed ultrasound shows promising potential as a new type of treatment. In this thesis, a wearable transcranial LIPUS treatment device is designed for mental health treatment. The flow chart of the design project can be summarized as three steps: 1) circuit design for the wearable LIPUS generator device; 2) transcranial headphone design for the previous LIPUS generator; and 3) verification and safety assessment.

In response to the needs of portable miniaturization and Internet of Things devices, we have designed a wearable LIPUS device that can be remotely controlled and viewed by a clinician. This wearable LIPUS device consists of an impedance transform module, a signal generator module, and a Bluetooth communication module. This fabricated LIPUS device generates LIPUS stimulation from 6.1 mW/cm^2 to 120 mW/cm^2 intensity, with center frequency at 1.5 MHz and repetition rate at 1 kHz with 20% duty cycle.

We have designed a new replaceable cap made of polyurethane rubber to cover the metal transducer. We have also investigated the best coupling agent. Three coupling agent materials were compared according to their acoustic transmission coefficient. Studies show that Milli-Q water is the best coupling agent among them, with a 39.76% transmission rate. For future study, we will focus on further miniaturizing the design for clinical use.

Although LIPUS has been shown to be a feasible treatment tool for neuromodulation with some much-encouraging evidence, safety assessment, and feasibility report for LIPUS in non-invasive neuromodulation have rarely been researched. The current study was designed to develop a therapeutic LIPUS headphone-style system and to explore the intensity diffusion and thermal profiling of the soft tissue inside the brain. We hypothesized that some ultrasonic energy enters the brain tissue through the skull, but the amplitude of the ultrasound signal is substantially attenuated when passing through the skull. To test this hypothesis, both simulation and *in-vitro* tests were conducted. The experimental results show that when low-intensity ultrasound is applied to the human brain, a small amount of ultrasonic stimulation can be received in the center of the brain with an insignificant temperature rise. The results indicate that our customized wearable LIPUS device can be used as a promising and emerging treatment approach for mental illness.

Future work can be divided into two aspects. First, we could focus on the miniaturized design of portable pulsed ultrasound treatment equipment. We could integrate the power supply system and the signal generation system into one chip. Only the impedance matching module and the Bluetooth module were designed as external discrete components. In the chip design, the signal transmission efficiency and miniaturization can be further optimized.

On the other hand, there is still much space for the development of LIPUS verification and clinical safety work. We can verify this by *in vitro* experiments using brain mimicking architecture or *in vivo* experiments by placing a head-mounted LIPUS therapy device on the animal's head. Clinical trials for humans will be a crucial step. We can also design a special LIPUS transducer so that ultrasound can stimulate a more substantial area at a lower intensity to achieve a better treatment effect.

Bibliography

[1] D.-. A. P. Association *et al.*, "Diagnostic and statistical manual of mental disorders," *Arlington: American Psychiatric Publishing*, 2013.

[2] W. H. Organization *et al.*, "Depression and other common mental disorders: Global health estimates," World Health Organization, Tech. Rep., 2017.

[3] A. Werner-Seidler, Y. Perry, A. L. Calear, J. M. Newby, and H. Christensen, "School-based depression and anxiety prevention programs for young people: A systematic review and meta-analysis," *Clinical psychology review*, vol. 51, pp. 30–47, 2017.

[4] S. M. Marcus, H. A. Flynn, F. C. Blow, and K. L. Barry, "Depressive symptoms among pregnant women screened in obstetrics settings," *Journal of women's health*, vol. 12, no. 4, pp. 373–380, 2003.

[5] J. Evans, J. Heron, H. Francomb, S. Oke, and J. Golding, "Cohort study of depressed mood during pregnancy and after childbirth," *Bmj*, vol. 323, no. 7307, pp. 257–260, 2001.

[6] G. J. Emslie, A. J. Rush, W. A. Weinberg, C. M. Gullion, J. Rintelmann, and C. W. Hughes, "Recurrence of major depressive disorder in hospitalized children and adolescents," *Journal of the American Academy of Child & Adolescent Psychiatry*, vol. 36, no. 6, pp. 785–792, 1997.

[7] L. R. Wulsin, G. E. Vaillant, and V. E. Wells, "A systematic review of the mortality of depression," *Psychosomatic medicine*, vol. 61, no. 1, pp. 6–17, 1999.

[8] S. B. Patten, J. V. Williams, D. H. Lavorato, J. L. Wang, K. McDonald, and A. G. Bulloch, "Major depression in canada: What has changed over the past 10 years?" *The Canadian Journal of Psychiatry*, vol. 61, no. 2, pp. 80–85, 2016.

[9] R. C. Kessler, S. Avenevoli, J. Costello, J. G. Green, M. J. Gruber, K. A. McLaughlin, M. Petukhova, N. A. Sampson, A. M. Zaslavsky, and K. R. Merikangas, "Severity of 12-month dsm-iv disorders in the national comorbidity survey replication adolescent supplement," *Archives of general psychiatry*, vol. 69, no. 4, pp. 381–389, 2012.

[10] G. Hasler, "Pathophysiology of depression: Do we have any solid evidence of interest to clinicians?" *World Psychiatry*, vol. 9, no. 3, pp. 155–161, 2010.

[11] C. Ménard, G. E. Hodes, and S. J. Russo, "Pathogenesis of depression: Insights from human and rodent studies," *Neuroscience*, vol. 321, pp. 138–162, 2016.

[12] J. J. Schildkraut, "The catecholamine hypothesis of affective disorders: A review of supporting evidence," *American journal of Psychiatry*, vol. 122, no. 5, pp. 509–522, 1965.

[13] G. Kempermann and G. Kronenberg, "Depressed new neurons?—adult hippocampal neurogenesis and a cellular plasticity hypothesis of major depression," *Biological psychiatry*, vol. 54, no. 5, pp. 499–503, 2003.

[14] S. Hitoshi, N. Maruta, M. Higashi, A. Kumar, N. Kato, and K. Ikenaka, "Antidepressant drugs reverse the loss of adult neural stem cells following chronic stress," *Journal of neuroscience research*, vol. 85, no. 16, pp. 3574–3585, 2007.

[15] R. S. Duman, G. R. Heninger, and E. J. Nestler, "A molecular and cellular theory of depression," *Archives of general psychiatry*, vol. 54, no. 7, pp. 597–606, 1997.

[16] M. Hamidi, W. C. Drevets, and J. L. Price, "Glial reduction in amygdala in major depressive disorder is due to oligodendrocytes," *Biological psychiatry*, vol. 55, no. 6, pp. 563–569, 2004.

[17] P. M. Plotsky, M. J. Owens, and C. B. Nemeroff, "Psychoneuroendocrinology of depression: Hypothalamic-pituitary-adrenal axis," *Psychiatric Clinics of North America*, vol. 21, no. 2, pp. 293–307, 1998.

[18] J. Jensen, *Depression and inflammation: The role of inflammatory biomarkers in the pathogenesis of depression*, 2019.

[19] V. WALIA, "Role of enzymes in the pathogenesis of depression," *Journal of Critical Reviews*, vol. 3, no. 2, p. 2016, 2016.

[20] Y. Bansal and A. Kuhad, "Mitochondrial dysfunction in depression," *Current neuropharmacology*, vol. 14, no. 6, pp. 610–618, 2016.

[21] H. G. Ruhé, N. S. Mason, and A. H. Schene, "Mood is indirectly related to serotonin, norepinephrine and dopamine levels in humans: A meta-analysis of monoamine depletion studies," *Molecular psychiatry*, vol. 12, no. 4, pp. 331–359, 2007.

[22] N. C. C. for Mental Health (UK *et al.*, "Depression: The treatment and management of depression in adults (updated edition)," British Psychological Society, 2010.

[23] A. J. Gelenberg, "A review of the current guidelines for depression treatment," *J Clin Psychiatry*, vol. 71, no. 7, e15, 2010.

[24] P. J. Carek, S. E. Laibstain, and S. M. Carek, "Exercise for the treatment of depression and anxiety," *The International Journal of Psychiatry in Medicine*, vol. 41, no. 1, pp. 15–28, 2011.

[25] G. E. Mead, W. Morley, P. Campbell, C. A. Greig, M. McMurdo, and D. A. Lawlor, "Exercise for depression," *Cochrane database of systematic reviews*, no. 4, 2008.

[26] E. D. Freis, "Mental depression in hypertensive patients treated for long periods with large doses of reserpine," *New England Journal of Medicine*, vol. 251, no. 25, pp. 1006–1008, 1954.

[27] G. E. Murphy, A. D. Simons, R. D. Wetzel, and P. J. Lustman, "Cognitive therapy and pharmacotherapy: Singly and together in the treatment of depression," *Archives of general psychiatry*, vol. 41, no. 1, pp. 33–41, 1984.

[28] A. J. Rush, M. H. Trivedi, S. R. Wisniewski, A. A. Nierenberg, J. W. Stewart, D. Warden, G. Niederehe, M. E. Thase, P. W. Lavori, B. D. Lebowitz, *et al.*, "Acute and longer-term outcomes in depressed outpatients requiring one or several treatment steps: A star* d report," *American Journal of Psychiatry*, vol. 163, no. 11, pp. 1905–1917, 2006.

[29] N. I. for Clinical Excellence, G. Britain, *et al.*, "Depression: Management of depression in primary and secondary care," 2004.

[30] F Rachid and G Bertschy, "Safety and efficacy of repetitive transcranial magnetic stimulation in the treatment of depression: A critical appraisal of the last 10 years," *Neurophysiologie Clinique/Clinical Neurophysiology*, vol. 36, no. 3, pp. 157–183, 2006.

[31] R. J. DeRubeis, G. J. Siegle, and S. D. Hollon, "Cognitive therapy versus medication for depression: Treatment outcomes and neural mechanisms," *Nature Reviews Neuroscience*, vol. 9, no. 10, pp. 788–796, 2008.

[32] J. Siddique, J. Y. Chung, C. H. Brown, and J. Miranda, "Comparative effectiveness of medication versus cognitive-behavioral therapy in a randomized controlled trial of low-income young minority women with depression.," *Journal of consulting and clinical psychology*, vol. 80, no. 6, p. 995, 2012.

[33] S. Pampallona, P. Bollini, G. Tibaldi, B. Kupelnick, and C. Munizza, "Combined pharmacotherapy and psychological treatment for depression: A systematic review," *Archives of general psychiatry*, vol. 61, no. 7, pp. 714–719, 2004.

[34] L. L. Carpenter, "Neurostimulation in resistant depression," *Journal of Psychopharmacology*, vol. 20, no. 3_suppl, pp. 35–40, 2006.

[35] T. G. Bolwig, "Putative common pathways in therapeutic brain stimulation for affective disorders," *CNS spectrums*, vol. 8, no. 7, pp. 490–495, 2003.

[36] R. Abrams, *Electroconvulsive therapy*. Oxford University Press, 2002.

[37] X. Li, Z. Nahas, F. A. Kozel, B. Anderson, D. E. Bohning, and M. S. George, "Acute left prefrontal transcranial magnetic stimulation in depressed patients is associated with immediately increased activity in prefrontal cortical as well as subcortical regions," *Biological psychiatry*, vol. 55, no. 9, pp. 882–890, 2004.

[38] S. H. Lisanby, B. Luber, T. E. Schlaepfer, and H. A. Sackeim, "Safety and feasibility of magnetic seizure therapy (mst) in major depression: Randomized within-subject comparison with electroconvulsive therapy," *Neuropsychopharmacology*, vol. 28, no. 10, pp. 1852–1865, 2003.

[39] C. B. Nemeroff, H. S. Mayberg, S. E. Krahl, J. McNamara, A. Frazer, T. R. Henry, M. S. George, D. S. Charney, and S. K. Brannan, "Vns therapy in treatment-resistant depression: Clinical evidence and putative neurobiological mechanisms," *Neuropsychopharmacology*, vol. 31, no. 7, pp. 1345–1355, 2006.

[40] S. J. Rizvi, M. Donovan, P. Giacobbe, F. Placenza, S. Rotzinger, and S. H. Kennedy, *Neurostimulation therapies for treatment resistant depression: A focus on vagus nerve stimulation and deep brain stimulation*, 2011.

[41] M. R. García, B. A. Pearlmutter, P. E. Wellstead, and R. H. Middleton, "A slow axon antidromic blockade hypothesis for tremor reduction via deep brain stimulation," *PloS one*, vol. 8, no. 9, 2013.

[42] A. Abosch and A. Lozano, "Stereotactic neurosurgery for movement disorders," *Canadian journal of neurological sciences*, vol. 30, no. S1, S72–S82, 2003.

[43] N. Webster, *Webster's ninth new collegiate dictionary*. Merriam-Webster, 1983.

[44] G. Ter Haar, "Therapeutic applications of ultrasound," *Progress in biophysics and molecular biology*, vol. 93, no. 1-3, pp. 111–129, 2007.

[45] M. Goudelin, B. Evrard, F. Dalmay, A. H. Padilla, C. Gonzalez, T. Lafon, T. Daix, A.-L. Fedou, B. François, and P. Vignon, "Diagnostic capability of a next-generation, ultra-miniaturized ultrasound system in patients with cardiopulmonary compromise assessed using basic critical care echocardiography," *Intensive care medicine*, vol. 44, no. 9, pp. 1579–1581, 2018.

[46] K. G. Baker, V. J. Robertson, and F. A. Duck, "A review of therapeutic ultrasound: Biophysical effects," *Physical therapy*, vol. 81, no. 7, pp. 1351–1358, 2001.

[47] X. Jiang, O. Savchenko, Y. Li, S. Qi, T. Yang, W. Zhang, and J. Chen, "A review of low-intensity pulsed ultrasound for therapeutic applications," *IEEE Transactions on Biomedical Engineering*, vol. 66, no. 10, pp. 2704–2718, 2018.

[48] R. W. Wood and A. L. Loomis, "Xxxviii. the physical and biological effects of high-frequency sound-waves of great intensity," *The London, Edinburgh, and Dublin philosophical magazine and journal of science*, vol. 4, no. 22, pp. 417–436, 1927.

[49] E. N. Harvey and A. L. Loomis, *High frequency sound waves of small intensity and their biological effects*, 1928.

[50] T. Watson and S. R. Young, "Therapeutic ultrasound," *Watson T. Electrotherapy Evidence-Based Practice. Edinburgh, UK: Churchill Livingstone*, pp. 179–200, 2008.

[51] J. A. Gallo, D. O. Draper, L. T. Brody, and G. W. Fellingham, "A comparison of human muscle temperature increases during 3-mhz continuous and pulsed ultrasound with equivalent temporal average intensities," *Journal of Orthopaedic & Sports Physical Therapy*, vol. 34, no. 7, pp. 395–401, 2004.

[52] M. H. Repacholi, M. Gandolfo, and A. Rindi, *Ultrasound: medical applications, biological effects, and hazard potential*. Springer Science & Business Media, 2012.

[53] J. A. Zagzebski, *Essentials of ultrasound physics*. Mosby, 1996.

[54] A. Khanna, R. T. Nelmes, N. Gougoulias, N. Maffulli, and J. Gray, "The effects of lipus on soft-tissue healing: A review of literature," *British medical bulletin*, vol. 89, no. 1, pp. 169–182, 2009.

[55] A. Mortimer and M Dyson, "The effect of therapeutic ultrasound on calcium uptake in fibroblasts," *Ultrasound in Medicine and Biology*, vol. 14, no. 6, pp. 499–506, 1988.

[56] K. N. Malizos, M. E. Hantes, V. Protopappas, and A. Papachristos, "Low-intensity pulsed ultrasound for bone healing: An overview," *Injury*, vol. 37, no. 1, S56–S62, 2006.

[57] F. Ahmadi, I. V. McLoughlin, S. Chauhan, and G. Ter-Haar, "Bio-effects and safety of low-intensity, low-frequency ultrasonic exposure," *Progress in biophysics and molecular biology*, vol. 108, no. 3, pp. 119–138, 2012.

[58] T. Nakamura, S. Fujihara, K. Yamamoto-Nagata, T. Katsura, T. Inubushi, and E. Tanaka, "Low-intensity pulsed ultrasound reduces the inflammatory activity of synovitis," *Annals of biomedical engineering*, vol. 39, no. 12, p. 2964, 2011.

[59] C Corradi and A Cozzolino, "The action of ultrasound on the evolution of an experimental fracture in rabbits," *Minerva Ortop*, vol. 55, pp. 44–5, 1952.

[60] V. Frenkel, *Therapeutic ultrasound: Mechanisms to applications*. Nova Science Publishers, 2011.

[61] C. S. Enwemeka, O. Rodriguez, and S. Mendosa, "The biomechanical effects of low-intensity ultrasound on healing tendons," *Ultrasound in Medicine and Biology*, vol. 16, no. 8, pp. 801–807, 1990.

[62] J. W. GERSTEN, "Effect of ultrasound on tendon extensibility," *American Journal of Physical Medicine & Rehabilitation*, vol. 34, no. 2, pp. 362–369, 1955.

[63] M Roberts, J. Rutherford, and D Harris, "The effect of ultrasound on flexor tendon repairs in the rabbit," *Hand*, no. 1, pp. 17–20, 1982.

[64] S. Warden, B. Metcalf, Z. Kiss, J. Cook, C. Purdam, K. L. Bennell, and K. Crossley, "Low-intensity pulsed ultrasound for chronic patellar tendinopathy: A randomized, double-blind, placebo-controlled trial," *Rheumatology*, vol. 47, no. 4, pp. 467–471, 2008.

[65] J. G. Tidball and S. A. Villalta, "Regulatory interactions between muscle and the immune system during muscle regeneration," *American Journal of Physiology-Regulatory, Integrative and Comparative Physiology*, vol. 298, no. 5, R1173–R1187, 2010.

[66] M. Kim, C.-H. Kim, H. H. Jung, S. J. Kim, and J. W. Chang, "Treatment of major depressive disorder via magnetic resonance–guided focused ultrasound surgery," *Biological psychiatry*, vol. 83, no. 1, e17–e18, 2018.

[67] X. Li, F. Weng, W. Sun, R. Liu, and H. Xu, "Preliminary research on depression treatment: Combination of transcranial magnetic stimulation and mri-guided low-intensity focused ultrasound pulsation," *Journal of Medical Imaging and Health Informatics*, vol. 10, no. 3, pp. 677–680, 2020.

[68] W. J. Tyler, Y. Tufail, M. Finsterwald, M. L. Tauchmann, E. J. Olson, and C. Majestic, "Remote excitation of neuronal circuits using low-intensity, low-frequency ultrasound," *PloS one*, vol. 3, no. 10, 2008.

[69] C.-M. Chen, C.-T. Wu, T.-H. Yang, S.-H. Liu, and F.-Y. Yang, "Preventive effect of low intensity pulsed ultrasound against experimental cerebral ischemia/reperfusion injury via apoptosis reduction and brain-derived neurotrophic factor induction," *Scientific reports*, vol. 8, no. 1, pp. 1–11, 2018.

[70] S.-L. Huang, C.-W. Chang, Y.-H. Lee, and F.-Y. Yang, "Protective effect of low-intensity pulsed ultrasound on memory impairment and brain damage in a rat model of vascular dementia," *Radiology*, vol. 282, no. 1, pp. 113–122, 2017.

[71] W.-S. Su, C.-H. Wu, S.-F. Chen, and F.-Y. Yang, "Low-intensity pulsed ultrasound improves behavioral and histological outcomes after experimental traumatic brain injury," *Scientific reports*, vol. 7, no. 1, pp. 1–10, 2017.

[72] H. Guo, "Treating depression with ultrasound: An exploratory study," Master's thesis, University of Alberta, 116 St. and 85 Ave., Edmonton, AB, Canada T6G 2R3, Jun. 2016.

[73] Z Qiu, S Kala, J Guo, Q Xian, J Zhu, and L Sun, "Non-invasive and selective brain stimulation by ultrasound via activation of mechanosensitive ion channels," *Brain Stimulation: Basic, Translational, and Clinical Research in Neuromodulation*, vol. 12, no. 2, p. 475, 2019.

[74] E Kim, E Anguluan, and J Kim, "Portable wireless transcranial ultrasound brain stimulation for freely behaving small animals," *Brain Stimulation: Basic, Translational, and Clinical Research in Neuromodulation*, vol. 12, no. 2, p. 570, 2019.

[75] V. Erfani, K. Goodarzi, M. Ebrahimi, and M. Roozbahani, "The effects of ultrasound, infrasound, and electroconvulsive stimulations on anxiety-like behavior in mice," *International Journal of Psychology (IPA)*, 2020.

[76] S. J. Reznik, J Sanguinetti, and J. Allen, "Transcranial ultrasound (tus) reduces worry in a five-day double-blind pilot study," *Change*, vol. 6, no. 8, p. 10, 2017.

[77] M. Legrand, L. Galineau, A. Novell, B. Planchez, B. Brizard, S. Leman, C. Tauber, J.-M. Escoffre, A. Lefèvre, P. Gosset, *et al.*, "Efficacy of chronic ultrasound neurostimulation on behaviors and distributed brain metabolism in depressive-like mice," *BioRxiv*, p. 813 006, 2019.

[78] D. L. Miller, N. B. Smith, M. R. Bailey, G. J. Czarnota, K. Hynynen, I. R. S. Makin, and B. C. of the American Institute of Ultrasound in Medicine, "Overview of therapeutic ultrasound applications and safety considerations," *Journal of ultrasound in medicine*, vol. 31, no. 4, pp. 623–634, 2012.

[79] S. Qi, Y. Li, W. Zhang, and J. Chen, "Design of a novel wearable lipus treatment device for mental health treatment," in *2018 40th Annual International Conference of the IEEE Engineering in Medicine and Biology Society (EMBC)*, IEEE, 2018, pp. 6052–6055.

[80] J. Blitz, "Fundamentals of ultrasonics," 1967.

[81] W. T. Ang, C. Scurtescu, W. Hoy, T. El-Bialy, Y. Y. Tsui, and J. Chen, "Design and implementation of therapeutic ultrasound generating circuit for dental tissue formation and tooth-root healing," *IEEE Transactions on biomedical circuits and Systems*, vol. 4, no. 1, pp. 49–61, 2009.

[82] T. Eriksson, S. Dixon, and S. Ramadas, "Flexural mode metal cap transducer design for specific frequency air coupled ultrasound generation," in *2013 IEEE International Ultrasonics Symposium (IUS)*, IEEE, 2013, pp. 1602–1605.

[83] R. A. Casarotto, J. C. Adamowski, F. Fallopa, and F. Bacanelli, "Coupling agents in therapeutic ultrasound: Acoustic and thermal behavior," *Archives of physical medicine and rehabilitation*, vol. 85, no. 1, pp. 162–165, 2004.

[84] P. K. Garu and T. K. Chaki, "Acoustic & mechanical properties of neoprene rubber for encapsulation of underwater transducers," *International Journal of Scientific Engineering and Technology*, vol. 1, no. 5, pp. 231–237, 2012.

[85] P. H. Mott, C. M. Roland, and R. D. Corsaro, "Acoustic and dynamic mechanical properties of a polyurethane rubber," *The Journal of the Acoustical Society of America*, vol. 111, no. 4, pp. 1782–1790, 2002.

[86] Y. Sun and X. Ye, "Enhancement or reduction of sonochemical activity of pulsed ultrasound compared to continuous ultrasound at 20 khz?" *Molecules*, vol. 18, no. 5, pp. 4858–4867, 2013.

[87] B. E. Treeby and B. T. Cox, "K-wave: Matlab toolbox for the simulation and reconstruction of photoacoustic wave fields," *Journal of biomedical optics*, vol. 15, no. 2, p. 021 314, 2010.

[88] D. White, F. Duck, A. Fairhead, L. Rothenberg, A Shaw, J. Zagzebski, and M Zankl, "Tissue substitutes, phantoms and computational modelling in medical ultrasound," *ICRU Report*, 1998.

[89] M. O. Culjat, D. Goldenberg, P. Tewari, and R. S. Singh, "A review of tissue substitutes for ultrasound imaging," *Ultrasound in medicine & biology*, vol. 36, no. 6, pp. 861–873, 2010.

[90] S. M. Blinkov and I. I. Glezer, *The human brain in figures and tables: a quantitative handbook*. Basic Books, 1968.

[91] P. S. Hariqbal Singh, *Atlas of Human Anatomy on MRI: Brain, Chest & Abdomen*. JP Medical Ltd, 2017.

[92] S. Ma, L. J. Baillie, and M. D. Stringer, "Reappraising the surface anatomy of the pterion and its relationship to the middle meningeal artery," *Clinical Anatomy*, vol. 25, no. 3, pp. 330–339, 2012.

[93] E. M. Lillie, J. E. Urban, S. K. Lynch, A. A. Weaver, and J. D. Stitzel, "Evaluation of skull cortical thickness changes with age and sex from computed tomography scans," *Journal of Bone and Mineral Research*, vol. 31, no. 2, pp. 299–307, 2016.

[94] A. C1055-03, *Standard guide for heated system surface conditions that produce contact burn injuries*, 2014.

Appendix A: Input Impedance of an L-matching Network

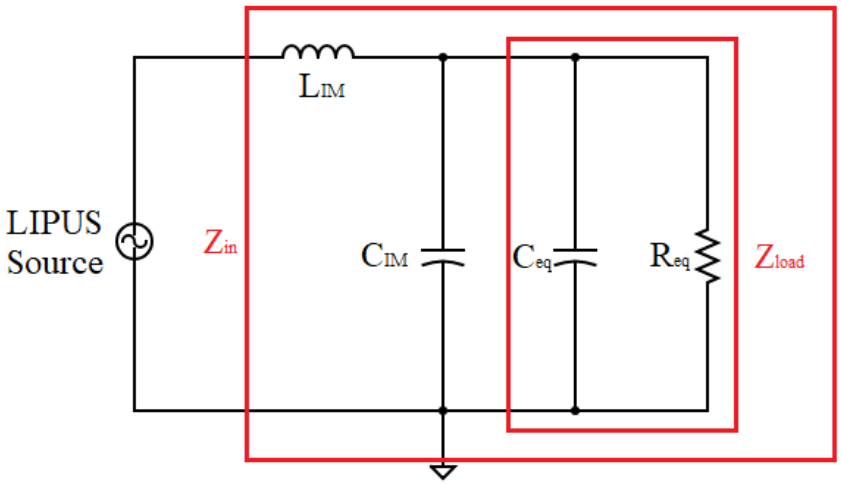

Figure A.1: An l-matching network consisting of an inductor, a conductor and the load.

In Figure A.1, the subscript "IM" denotes impedance matching, while "eq" stands for equivalent. The l-matching network L_{IM}, C_{IM} and load Z_{load} forms the entire input impedance Z_{in}. Two capacitors C_{IM} and C_{eq} are connected in parallel with an equivalent resistor R_{eq} and then in series with an inductor L_{IM}, which can be presented as the following equation.

$$\begin{aligned} Z_{in} &= j\omega L_{IM} + \frac{1}{j\omega C_{IM}} || \frac{1}{j\omega C_{eq}} || R_{eq} \\ &= j\omega L_{IM} + \frac{1}{j\omega (C_{IM} + C_{eq})} || R_{eq} \end{aligned} \tag{A.1}$$

The derivation of the input impedance is as follows:

$$
\begin{aligned}
Z_{in} &= j\omega L_{IM} + \frac{1}{j\omega(C)} || R_{eq} \\
&= j\omega L_{IM} + \frac{\frac{R_{eq}}{j\omega C}}{\frac{1}{j\omega C} + R_{eq}} \\
&= j\omega L_{IM} + \frac{R_{eq}}{1 + j\omega C R_{eq}} \\
&= \frac{R_{eq} + j\omega(L_{IM} - R_{eq}^2 C(1 - \omega^2 L_{IM} C))}{1 + \omega^2 C^2 R_{eq}^2}
\end{aligned}
\tag{A.2}
$$

where $C = C_{IM} + C_{eq}$ is used to simplify calculations. The final equation is:

$$
Z_{in} = \frac{R_{eq} + j\omega(L_{IM} - R_{eq}^2 (C_{IM} + C_{eq})(1 - \omega^2 L_{IM}(C_{IM} + C_{eq})))}{1 + \omega^2 (C_{IM} + C_{eq})^2 R_{eq}^2} \tag{A.3}
$$

Appendix B: Serial Interface Code for the Micro Controller

B.1 Description

The following code is the main code used to drive the microcontroller ATmega328p created by Atmel in the megaAVR family. The 1.5 MHz square waves are generated by a 6 MHz Oscillator with two frequency dividers. In this code, a low-energy Bluetooth module BC118 receives the command from the phone application via the UART communication protocol. The command consists of the duration and the intensity of the LIPUS signal. Based on the duration time, pin PB0 will generate a 1 kHz square wave. By multiplying the 1.5 MHz square wave signal and the 1 kHz square wave signal, we successfully obtained the baseline signal with pulses. The other two pins PB1 and PB2 will generate the corresponding signal to two 8-bit digital potentiometers, which will turn the power amplifier module to the desired intensity.

This program is written with Arduino Programming Language and compiled in Arduino IDE (version 1.8.3).

B.2 Code

Listing B.1: Code for the main() Function

```
/*************************************************************
 * This module use BC118 BLE module on the BLE Mate 2 board by
 * SparkFun electronics to communicate with iPhone or Android
 * Apps using Bluetooth communication.
 * This UltrasoundMainControl code is created by Shi-ang Qi
 * Code developed in Arduino 1.8.3
*************************************************************/
#include <SoftwareSerial.h>
#include <SparkFunBLEMate2.h>
```

```
#include <SPI.h>

// BLE Mate3 OR BC118
// GND - GND
// CTS - GND
// VIN - 3.3v
// TXO - 2
// RXI - 10
// DTR - GND

// SCK - 13
// MOSI - 11
// Slave Select Pin/CS - 9
// Start Signal - 8
// 1kHz Signal - 3

int bluetoothTx = 2;
int bluetoothRx = 10;

// create a softwareSerial port object and pass that to the BLEMate2 constructor

SoftwareSerial bluetoothSerial(bluetoothTx, bluetoothRx);

BLEMate2 BTModu(&bluetoothSerial);

//  peripheral mode


boolean central = false;

void setup()
{

  Serial.begin(9600);
  // This is the BC118 default baud rate.
  bluetoothSerial.begin(9600);



  // Regarding function return values: most functions that interact with the
  //  BC118 will return BLEMate2::opResult values. The possible values here
  //  are:
  //  REMOTE_ERROR - No remote devices exist.
  //  INVALID_PARAM - You've called the function with an invalid parameter.
  //  TIMEOUT_ERROR - The BC118 failed to respond to the command in a timely
  //                   manner; timely is redefined for each command.
  //  MODULE_ERROR - The BC118 didn't like the command string it received.
  //                 This will probably only occur when you attempt to send
  //                 commands and parameters outside the built-ins.
  //  SUCCESS - What it says.

  // Reset is a blocking function which gives the BC118 a few seconds to reset.
  //  After a reset, the module will return to whatever settings are in
  //  non-volatile memory. One other *super* important thing it does is issue
  //  the "SCN OFF" command after the reset is completed. Why is this important?
  //  Because if the device is in central mode, it *will* be scanning on reset.
  //  No way to change that. The text traffic generated by the scanning will
  //  interfere with the firmware on the Arduino properly identifying response
  //  strings from the BC118.
  if (BTModu.reset() != BLEMate2::SUCCESS)
  {

    Serial.println("Module reset error!");
    while (1);
  }

  // restore() resets the module to factory defaults; you'll need to perform
  //  a writeConfig() and reset() to make those settings take effect. We don't
```

```
  //  do that automatically because there may be things the user wants to
  //  change before committing the settings to non-volatile memory and
  //  resetting.
  if (BTModu.restore() != BLEMate2::SUCCESS)
  {

    Serial.println("Module restore error!");
    while (1);
  }
  // writeConfig() stores the current settings in non-volatile memory, so they
  //  will be in place on the next reboot of the module. Note that some, but
  //  not all, settings changes require a reboot. It's probably in general best
  //  to write/reset when changing anything.
  if (BTModu.writeConfig() != BLEMate2::SUCCESS)
  {

    Serial.println("Module write config error!");
    while (1);
  }
  // One more reset, to make the changes take effect.
  if (BTModu.reset() != BLEMate2::SUCCESS)
  {

    Serial.println("Second module reset error!");
    while (1);
  }


    setupPeripheralExample();
    digiPotInit();
    repetitionInit();

}

void loop()
{
 // buffer for RCV data
  static String fullBuffer;

  // buffer for bluetooth Data
  static String inputBuffer;

  static long lastRXTime = millis();

  // if more than 1000
  //  milliseconds has elapsed since last receive
  // parse the command from Iphone apps
  if (lastRXTime + 1000 < millis())
  {
    if (fullBuffer != "")
    {
      Serial.println(fullBuffer);
      fullBuffer = "";
    }
  }

   // read data from bluetooth
   while (bluetoothSerial.available() > 0)
    {
      inputBuffer.concat((char)bluetoothSerial.read());
      lastRXTime = millis();
    }

   // check to see if the string
   // and data looks like this:
   // RCV=20 char max msg\n\r

   // if yes copy it to fullBuffer array
```

```
    if (inputBuffer.endsWith("\n\r"))
    {

     if (inputBuffer.startsWith("RCV="))
      {
        Serial.println("This is a RCV");
       // copy to RCV buffer
        inputBuffer.trim(); // Remove \n\r from end.
        inputBuffer.remove(0,4); // Remove RCV= from front.
        fullBuffer += inputBuffer;
        inputBuffer = "";
        digiPotChange(fullBuffer.toInt());
      }
      else
      {
        inputBuffer = "";
      }
    }

  delay(100);
}

void digiPotInit()
{
  //signal control the digital potentiometer
  #define CS_signal 3
  #define CLK_signal 4
  #define MOSI_signal 5

  pinMode(MOSI_signal,OUTPUT);
  pinMode(CS_signal,OUTPUT);
  pinMode(CLK_signal,OUTPUT);

  digitalWrite(CS_signal,HIGH);
}

void repetitionInit()
{
  pinMode(11,OUTPUT);
  digitalWrite(11,HIGH);
}


//set the resistance value based on the bluetooth input
void digiPotChange(int numberUp)
{
  // Set the resistance value to 0, then increase the resistance numberUp times.
  digitalWrite(MOSI_signal,LOW);
  for (int i = 63; i>0; --i){
    digitalWrite(CLK_signal,HIGH);
    delay(20);
    digitalWrite(CLK_signal,LOW);
  }

  Serial.print("Resistance increase ");
  Serial.print(numberUp);
  Serial.println(" Ohm");

  digitalWrite(MOSI_signal,HIGH);
  for (int i = 0; i <numberUp; i++){
    digitalWrite(CLK_signal,HIGH);
    delay(20);
    digitalWrite(CLK_signal,LOW);
  }
}

// The default settings are good enough for the peripheral example; just to
```

```
//  be on the safe side, we'll check the amICentral() function and do a r/w/r
//  if we're in central mode instead of peripheral mode.
void setupPeripheralExample()
{
  boolean inCentralMode = false;
  // A word here on amCentral: amCentral's parameter is passed by reference, so
  //  the answer to the question "am I in central mode" is handed back as the
  //  value in the boolean passed to it when it is called. The reason for this
  //  is the allow the user to check the return value and determine if a module
  //  error occurred: should I trust the answer or is there something larger
  //  wrong than merely being in the wrong mode?
  BTModu.amCentral(inCentralMode);
  if (inCentralMode)
  {
    BTModu.BLEPeripheral();
    BTModu.BLEAdvertise();
  }

  // There are a few more advance settings we'll probably, but not definitely,
  //  want to tweak before we reset the device.

  // The CCON parameter will enable advertising immediately after a disconnect.
  BTModu.stdSetParam("CCON", "ON");
  // The ADVP parameter controls the advertising rate. Can be FAST or SLOW.
  BTModu.stdSetParam("ADVP", "FAST");
  // The ADVT parameter controls the timeout before advertising stops. Can be
  //  0 (for never) to 4260 (71min); integer value, in seconds.
  BTModu.stdSetParam("ADVT", "0");
  // The ADDR parameter controls the devices we'll allow to connect to us.
  //  All zeroes is "anyone".
  BTModu.stdSetParam("ADDR", "000000000000");

  BTModu.writeConfig();
  BTModu.reset();

  // We're set up to allow anything to connect to us now.
}
```

Appendix C: Addition Figures of the LIPUS System

C.1 PCB Boards

Figure C.1 shows the two-PCB-board layout design, including both a mainboard and two driver boards (impedance matching boards). The mainboard contains the Bluetooth module, microcontroller, pulsed square signal generator, and supplied voltage amplitude control. Two driver boards, containing impedance matching circuitry, are placed inside the headband next to the transducers to drive the transducers. Figure C.2 is the photograph of the fabricated PCB boards.

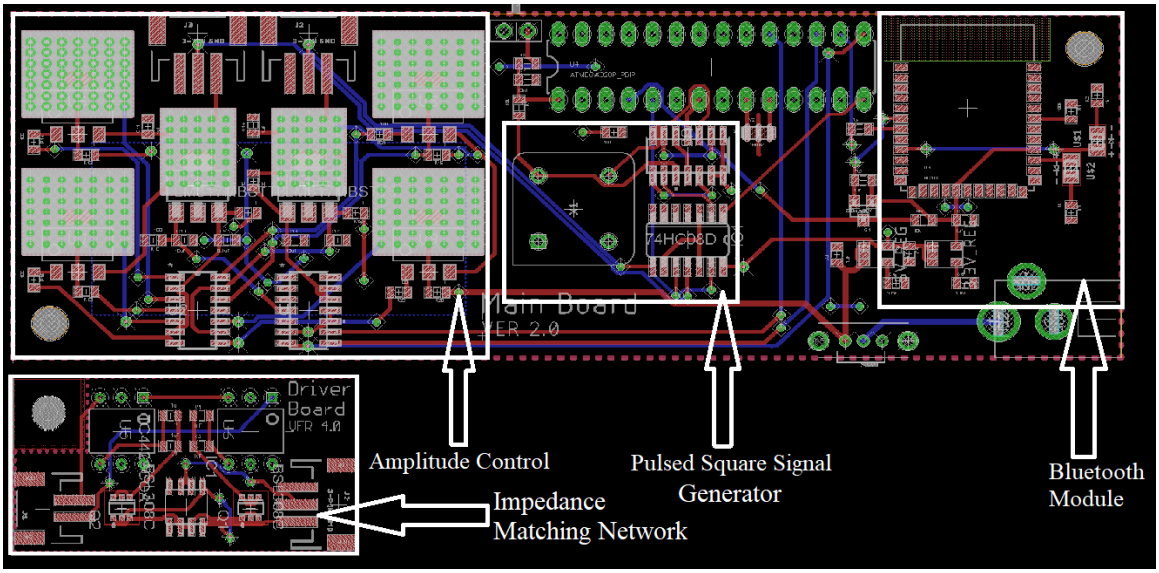

Figure C.1: PCB layout for main board (top) and drive board / impedance matching board (oower left corner) proposed in [79].

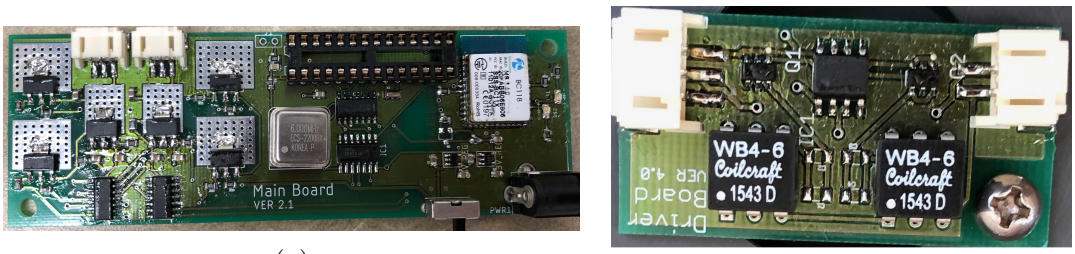

(a) (b)

Figure C.2: Photograph of the fabricated PCB board. (a) Main board; (b) drive board/ impedance matching board.

C.2 Box and Other Components

Figure C.3 is the perspective view, front view, right view, and top view of the wearable LIPUS box.

C.3 Software Interface

Figure C.4 is the software we developed to control the portable transcranial LIPUS device. It is developed based on the open-source software (MelodySmart) on the Android platform. The prescription we can enter from the smartphone includes the duration of the stimulation time and the LIPUS intensity.

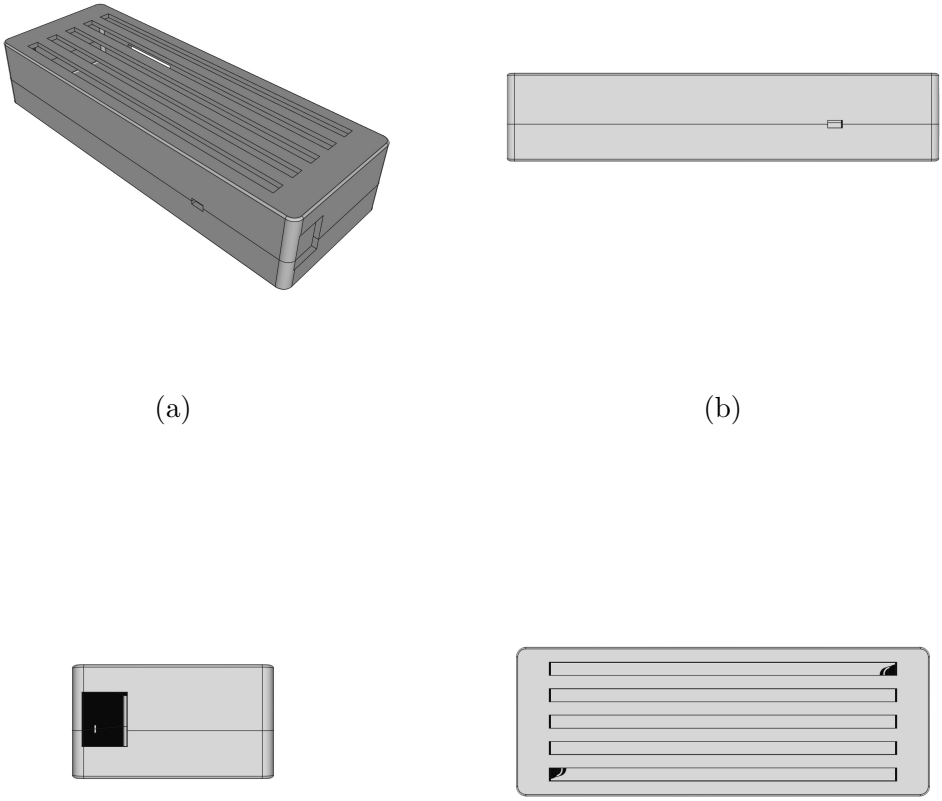

(a) (b)

(c) (d)

Figure C.3: The model diagram of the LIPUS box. (a) Perspective view; (b) front view; (c) right view; (d) top view.

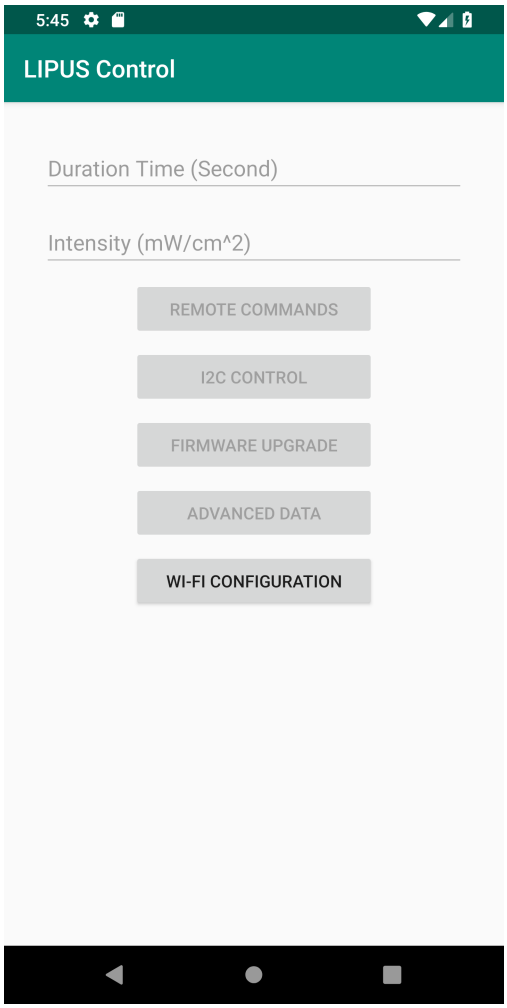

Figure C.4: Interface of the Android software.